Experimental investigation of wave attenuation by mangrove forests with submerged canopies

Zhang, Rong; Chen, Yongping; Lei, Jiaxin; Zhou, Xin; Yao, Peng; Stive, Marcel J.F.

DOI
10.1016/j.coastaleng.2023.104403

Publication date
2023

Document Version
Final published version

Published in
Coastal Engineering

Citation (APA)
Zhang, R., Chen, Y., Lei, J., Zhou, X., Yao, P., & Stive, M. J. F. (2023). Experimental investigation of wave attenuation by mangrove forests with submerged canopies. *Coastal Engineering*, *186*, Article 104403. https://doi.org/10.1016/j.coastaleng.2023.104403

Coastal Engineering 186 (2023) 104403

Contents lists available at ScienceDirect

Coastal Engineering

journal homepage: www.elsevier.com/locate/coastaleng

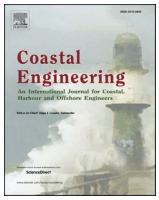

Experimental investigation of wave attenuation by mangrove forests with submerged canopies

Rong Zhang [a,b,f], Yongping Chen [a,b,*], Jiaxin Lei [b], Xin Zhou [b,c,e], Peng Yao [a,b], Marcel J.F. Stive [d]

[a] The National Key Laboratory of Water Disaster Prevention, Hohai University, Nanjing, China
[b] College of Harbour, Coastal and Offshore Engineering, Hohai University, Nanjing, China
[c] Second Institute of Oceanography, Ministry of Natural Resources, Hangzhou, China
[d] Department of Hydraulic Engineering, Delft University of Technology, Delft, the Netherlands
[e] Key Laboratory of Ocean Space Resource Management Technology, Ministry of Natural Resources, Hangzhou, China
[f] State Environmental Protection Key Laboratory of Marine Ecosystem Restoration, Dalian, China

ARTICLE INFO

Keywords:
Wave attenuation
Submerged mangrove canopies
Wave damping factor
Drag coefficient
Experimental analysis

ABSTRACT

Mangroves can function as a 'bio-shield' to protect coastal communities from harsh environments because of their strong ability to attenuate wave energy. However, as mangroves are usually oversimplified as rigid cylinders in antecedent studies, the effects of complex mangrove morphology on wave attenuation have not been well researched. Although increasing attention has been paid to the wave dissipation induced by varying mangrove morphologies, most of them focus on the bottom trunk and root components of mature mangrove trees. There are few investigations about the contributions of the canopies of young saplings and/or short species to wave attenuation. To bridge this knowledge gap, a series of laboratory experiments under regular waves were conducted to examine the hydrodynamic variations affected by varying mangrove morphology configurations. Three water depths were considered to explore the influences of the vertical-varying submerged volume of mangroves when the artificial mangrove models are submerged, nearly emergent, and fully emergent. The mangrove forest model is 2 m long at a 1:10 scale. Three mangrove configurations, i.e. with no canopy, sparse canopy, and dense canopy were applied and compared to isolate the wave attenuation contributed by mangrove canopies. The results highlight the wave energy attenuation attributed to the canopy density. A linear correlation is found between the wave damping factor and a new variable named hydraulic submerged volume index (HSVI). The bulk drag coefficient, including canopy effects, was calculated to characterize mangrove-induced wave attenuation when the mangrove canopy is submerged. The relationships between the bulk drag coefficient C_D and the characteristic hydraulic numbers (i.e., Reynolds number, Keulegan–Carpenter number, Ursell number) are discussed in detail. Consequently, new generic formulas of C_D were deduced considering the effects of the submerged canopy. The employment of new C_D formulas improves the reliability of the prediction of the wave attenuation ability by mangroves since the canopy effects are incorporated.

1. Introduction

Mangroves are one of the important inter-tidal wetland species that dwell at the interface between land and sea along tropical and subtropical coasts (Saenger, 2002). Mangrove forests have been recognized as a great resource that provides plenty of ecosystem services and benefits (Alongi, 2008; Menéndez et al., 2020; Gijsman et al., 2021). For instance, mangroves can sequestrate carbon in their soils, offer nursery grounds for unique ecosystems, support the coastal food chain, act as a buffer zone to attenuate incident wave energy, reduce flooding risks by decreasing storm surges, and stabilize beach topography through sediment retention (Massel et al., 1999; Alongi, 2002; Yanagisawa et al., 2010; Van Coppenolle et al., 2018). The interaction between water flow and vegetation dominates hydrodynamics, sedimentation, mass transfer, and biological processes (Mazda et al., 1997; Brinkman, 2006; Tang et al., 2015).

The presence of coastal vegetation, functioning as a first coastal buffer line, has been widely admitted to the damping of substantial wave energy, runup, overtopping, and storm surges (Othman, 1994; Mazda, 1997; Feagin et al., 2010; Horstman et al., 2014; Tang et al., 2017, 2019;

* Corresponding author. The National Key Laboratory of Water Disaster Prevention, Hohai University, Nanjing, China.
E-mail address: ypchen@hhu.edu.cn (Y. Chen).

https://doi.org/10.1016/j.coastaleng.2023.104403
Received 5 February 2023; Received in revised form 20 September 2023; Accepted 22 September 2023
Available online 23 September 2023

Tomiczek et al., 2020a; Chang and Mori, 2021; Temmerman et al., 2023). A vegetated foreshore can effectively alleviate wave attacks on sheltered infrastructures, for instance, reducing the dike failure risk by reducing wave overtopping and retarding flushing flow (Vuik et al., 2018; Pan et al., 2020). A hybrid coastal protection plan incorporating coastal vegetation with other coastal protection strategies, i.e. sea dike, beach nourishment, would enhance coastal resilience to natural hazards, and make the hybrid coastal protection more sustainable and financially attractive (Zhu et al., 2020; van Zelst et al., 2021; Pan et al., 2022). It has been observed that mangrove forests can attenuate wave energy 3–5 times more than the bare bottom (Mullarney et al., 2017). Even a narrow mangrove forest can afford substantial protection to coastal zones from waves (Massel et al., 1999; Gedan et al., 2011). Only a 100–200 m wide mangrove belt can attenuate wave height sufficiently and reduce the damage risk of the dykes behind the green belt (Othman, 1994; Phan et al., 2014). After extreme events (e.g., the Indian Ocean Tsunami, 2004; Super Typhoon Haiyan, 2013), field observation records confirm less property damage and fewer casualties of hamlets behind dense mangroves (Danielsen et al., 2005; Das and Vincent, 2009; Hashim et al., 2013; Dahdouh-Guebas et al., 2013). Teo et al. (2009) carried out numerical simulations to show that mangroves reduce wave energy and tsunami current velocities significantly. In addition, mangroves indirectly damp wave impacts through promoting sediment deposition and building up bed level. Therefore, mangroves contribute to increase the integrity and resilience of coasts, providing the coastal communities a long-lasting, flexible and adaptive protection measure to combat the accelerating sea level rise and harsher environment.

With the increasing pressure on mitigating coastal hazards and reducing consequently catastrophic losses, more effective and economical protection strategies are in urgent need. Hence, utilizing mangroves as a nature-based coastal protection solution has attracted increasing attention (Barbier, 2006; Spalding et al., 2014; Hespen et al., 2023). Mangrove forests serve as a 'bio-shield' in supplement to hard coastal protection infrastructures (e.g., sea walls and dykes), making a hybrid coastal protection plan more popular and greener (Borsje et al., 2011; Gedan et al., 2011; Schoonees et al., 2019; Yuanita et al., 2021). Furthermore, the increasing awareness of the coastal protection value of mangroves has incented the restoration and conservation of mangroves, to enhance coastal resilience and adaption ability to climate change (Menéndez et al., 2020; Gijsman et al., 2021; Lee et al., 2021).

The performance of mangroves in attenuating waves depends on hydrodynamic conditions (e.g., water depth, wave spectrum) and mangrove characteristics (e.g., biomechanics, spatial density, morphology). The wave height reduction rate per unit length of mangrove forest ranges from 0.2% m^{-1} to 2.37% m^{-1} (Mazda et al., 1997; Brinkman, 2006). The wave dissipation by mangroves is primarily due to the interaction between waves with submerged vegetation volume. Generally, mangrove morphology can be divided into three distinct layers, i.e., canopy, stem, and root. The shape of roots tapers off upward, and at the canopy height, branches and leaves thickly spread. The complex root system, together with the tree stem and the canopy forms a complex interwoven network above the forest floor. The vertical structures of mangroves affect wave attenuation remarkably, which is significantly varied with different species (Tanaka et al., 2007). In the literature, *Rhizophora Sp.* is shown to dissipate wave energy more effectively than other species because of dense prop roots (Hadi et al., 2003; Tanaka et al., 2007). The prop roots of *Rhizophora* grow deep into the clay to anchor the stem and withstand the hydraulic forces. The deeper prop root system of *Rhizophora* also retards erosion and prevents them from toppling (Othman, 1994).

The literature review indicates that the importance of mangrove vertical morphology on the wave attenuation has not been systematically investigated. Lou et al. (2018) investigated vertically varying vegetation density on wave-vegetation interactions through laboratory experiments. They found that the vertically-varying density effects on wave height reduction are significant under deep water waves. Strusínska-Correia et al. (2013) used parameterized mangrove trees made of cylinders distributed in different layers to mimic the real mangrove roots. Following the 3-D geometric mangrove model of prop root morphology proposed by Ohira et al. (2013), a few large-scale (1:7 to 1:16) laboratory experiments were carried out to investigate wave dynamics within complex mangrove prop roots using parametrized or 3D-printed mangrove models (Maza et al., 2017; Maza et al., 2019; Chang et al., 2019; Tomiczek et al., 2020b; Wang et al., 2022b; Chang et al., 2022). Moreover, in recent years some 1:2.1 near-prototype scale experiments (Bryant et al., 2022) and 1:1 prototype-scale experiments (Kelty et al., 2022) were employed to discuss the scale effects. Kelty et al. (2022) pointed out that it is necessary to rescale the Reynolds number when comparing different C_D-Re correlations obtained from reduced scale experiments. However, while the abovementioned studies focused on the frequently submerged prop roots and lower stems of mature mangroves, few researchers paid attention to the canopy of short young saplings and dwarf mangroves, which are possibly submerged under deep water scenarios. Based on a field observation in Vietnam, Mazda et al. (2006) found that when the submerged canopy volume increased with rising water level, the rate of wave reduction increased, which indicates the strong potential of wave dissipation ability by mangrove densely canopy. He et al. (2019) pointed out that when the water level reaches the canopy geometrical centroid, the wave attenuation is higher than conditions when the canopies are emergent or nearly emergent. Similarly, based on a prototype-scale flume tests, van Wesenbeeck et al. (2022) observed that willow forests strongly reduce wave heights by the branches of willows, but the leaves of the willows were found to contribute very limitedly to wave attenuation. However, through wave flume tests, van Hespen et al. (2021) measured drag properties of collected mangrove branch samples from the field site, and they found larger leaf size resulted in larger frontal area and larger drag forces. Therefore, besides the qualitative cognitions, there is still a lack of understanding about quantifying the contribution of submerged mangrove canopy to wave attenuation.

To understand the effects of complex mangrove morphology, especially the canopies, on wave attenuation is the primary aim of this study. In this study, we extend the existing laboratory database by investigating the effects of mangrove canopy on wave attenuation under fully submerged conditions. We found that a submerged canopy attenuates wave energy more effectively than submerged stems and roots. Such findings offer a reference to evaluate the impacts of the variations of mangrove canopies on wave attenuation, which can further guide replantation and restoration projects of mangrove forests.

This paper is organized as follows. In Section 2, the analytical solutions of wave attenuation by vegetation are described. Section 3 briefly describes the setup of flume experiments and the data analysis. Section 4 demonstrates the detailed results and discussion on wave attenuation induced by submerged mangrove canopy. The conclusions and outlook of this study are summarized in Section 5.

2. Theoretical background

2.1. Wave attenuation by vegetation

The wave decay by vegetation under regular waves is evaluated by the formulas (Eqs. (1)–(4)) proposed by Dalrymple et al. (1984), based on the conservation of wave energy flux:

$$\frac{\partial\left(Ec_g\right)}{\partial \mathrm{x}} = -\varepsilon_D \tag{1}$$

where E ($=1/8\rho g H^2$) is the total average wave energy per unit surface area, H is the wave height, c_g is the wave group velocity, x is the wave propagation distance along the vegetation field, ε_D is the wave energy flux dissipation rate. The wave energy dissipation per unit width ε_D is due to the drag force by the vegetation, expressed as

$$\varepsilon_D = \int_{-h}^{h_{vs}-h} \frac{1}{2}\rho C_D A u|u| \bullet u dz \tag{2}$$

where h_{vs} is the submerged height of a mangrove tree, A is the projected frontal area, C_D is the drag coefficient, u is the horizontal velocity due to wave motion.

Rewriting the solution of Eq. (1) in the form of wave transmission coefficient k_t as:

$$k_t = \frac{H_t}{H_0} = \frac{1}{1+\beta x} \tag{3}$$

where H_0 is the incident wave height without mangrove interferences, and H_t is the transmitted wave height, β [m^{-1}] is the wave damping factor obtained with

$$\beta = \frac{4}{9\pi} C_D \overline{D} N H_0 k \frac{\sinh^3(kh_{vs}) + 3\sinh(kh_{vs})}{(\sinh(2kh) + 2kh)\sinh(kh)} \tag{4}$$

where k is the wave number, $\overline{D}$ is the depth averaged projected area (i.e., for cylinder is the cylinder diameter d; for the mangrove tree, $\overline{D} = \frac{1}{h}\int_{-h}^{0} A(z)dz$), and N is the vegetation density per unit horizontal area. Once β is obtained by fitting Eq. (3) to measured wave height decay (WHD), C_D can be obtained by inverting Eq. (4), which is called a calibration method (Hu et al., 2014). To isolate the effects of the bottom, the side walls, and the seaward slope, the wave height reduction measured under bare bottom conditions is subtracted from the measured wave heights through artificial mangroves (Hu et al., 2014; Maza et al., 2019). Then, the damping coefficient induced purely by mangroves is obtained by extracting other wave energy sinks.

2.2. Characteristic scales

2.2.1. Characteristic hydraulic parameters

It has been found that the bulk drag coefficient C_D of vegetation is closely related to the Reynolds number (*Re*), Keulegan-Carpenter number (*KC*), and Ursell number (*Ur*) (Hu et al., 2014; Anderson and Smith, 2014; Veelen et al., 2020; Wang et al., 2021).

The Reynolds number (*Re*) is defined as:

$$Re = \frac{u_s l_s}{\nu} \tag{5}$$

where u_s is a characteristic velocity amplitude, l_s is a characteristic vegetation length scale, ν is the water kinematic viscosity.

The Keulegan-Carpenter number (*KC*) represents the relative partial excursion length:

$$KC = \frac{u_s T}{l_s} \tag{6}$$

where T is the wave period.

The Ursell number (*Ur*) indicates the nonlinearity of surface waves by the ratio of the wave steepness (H/L, where $L = \frac{gT^2}{2\pi}\tanh(kh)$ is the wave length) to the relative wavelength kh as:

$$U_r = 8\pi^3 \frac{H/L}{(kh)^3} \tag{7}$$

2.2.2. Characteristic velocity scale

Several uncertainties exist in properly choosing the characteristic length and velocity scale to define the *Re* and *KC* numbers. In most studies, the depth-averaged wave orbital velocity amplitude has been selected:

$$\overline{u} = \frac{\omega a}{kh} \tag{8}$$

where ω is the wave angular frequency, $a = 0.5H$.

Alternatively, u_s can also be defined as the maximum horizontal velocity at the top of the vegetation (Mendez et al., 1999; Anderson and Smith, 2014). Suzuki et al. (2019) found that permeability effects are prominent with high vegetation density, which lead to greater wave height reduction. For very dense vegetation patches, the velocity was enhanced over the submerged vegetation canopy due to flow contraction effects. Thus the seepage velocity is an additionally available choice of u_s.

2.2.3. Characteristic length scale

When the canopy part of mangroves is emergent, l_e is the diameter of stems, if not, l_e is the effective vegetation length. The effective vegetation length l_e is defined as:

$$l_e = \frac{SV}{A_f} \tag{9}$$

where A_f is the frontal projected area per unit volume, and SV is the submerged solid volume of vegetation.

Another form of effective length scale proposed by Mazda et al. (1997) is an alternative length scale:

$$l_{ew} = \frac{V - SV}{A_f} \tag{10}$$

where V is the total underwater volume of the vegetation zone.

Cheng and Nguyen (2011) defined a vegetation-related hydraulic radius (r_v) as a function of the submerged volume fraction of vegetation SVF and the stem diameter d:

$$r_v = \frac{\pi}{4}\frac{1-\mathrm{SVF}}{\mathrm{SVF}} d \tag{11}$$

The different characteristic length scales were examined when comparing empirical correlations between the C_D coefficient with Reynolds number (*Re*), Keulegan-Carpenter number (*KC*), and Ursell number (*Ur*).

3. Methodology

To investigate the effects of submerged mangrove canopies on wave attenuation, we conducted a series of laboratory experiments in the wave flume at Hohai University. To highly mimic the natural mangrove morphology structures, we designed artificial mangrove models in the experiments. This section detail introduces the experimental setup and test hydraulic conditions, followed by the morphological features of mangroves in the field and the experiment.

3.1. Experimental setup

The physical experiments were conducted in the wave flume of the hydraulic lab at Hohai University. The wave flume is 85 m long, 1.0 m wide, and 1.5 m high. A wave maker was installed at the upstream end. At the other end, a wave absorption slope covered by dense polyurethane filter foam sheets is placed to eliminate wave reflection in the wave flume. In the literature, the scales of wave attenuation experiments by mangroves were between 1:1 and 1:16, fitting the size of available indoor wave flumes (Maza et al., 2017; Maza et al., 2019; Osorio et al., 2019; He et al., 2019; Tomiczek et al., 2020b; Chang et al., 2022; Bryant et al., 2022; Kelty et al., 2022; Tomiczek et al., 2023). In this study, we chose a 1:10 scale to fit the wave flume size. Experiments were carried out under regular waves. Following representative wave conditions for mangrove forests found in nature and reported in the literature (Bao, 2011; Brinkman, 2006; Maza et al., 2019), a wide and realistic range of wave conditions were selected with varying wave periods and wave heights. The Froude similarity was considered to calculate the hydraulic conditions on the laboratory scale. In this study, wave heights ranged from 0.04 m to 0.16 m, and wave periods are between 1.0 and 2.0 s. The

Table 1
Wave conditions and mangrove parameters.

	Scaled model (1:10)					Prototype				
Wave conditions	h (m)	H (m)	T (s)			h (m)	H (m)	T (s)		
	0.3	0.04–0.08	1.0–1.4			3	0.4–0.8	3.16–4.43		
	0.4	0.06–0.10	1.2–1.6			4	0.6–1.0	3.79–5.06		
	0.5	0.04–0.20	1.0–2.0			5	0.4–2.0	3.16–6.32		
Mangrove parameters	Canopy width W_c (m)	Canopy Height h_c (m)	Canopy volume V_c(m^3)			Canopy width W_c (m)	Canopy Height h_c (m)	Canopy volume V_c (m^3)		
	0.145	0.17	sparse:5×10^{-5} dense : 10^{-4}			1.45	1.70	sparse: 5×10^{-2} dense : 10^{-1}		
	Branch diameter (m)	Branch length (m)	Twig diameter (m)	Twig length (m)		Branch diameter (m)	Branch length (m)	Twig diameter (m)	Twig length (m)	
	0.0017	0.17	0.0011	0.079		0.017	1.70	0.011	0.79	
	Stem diameter	Stem height	Stem density			Stem diameter	Stem height	Stem density		
	DBH[a](m)	h_v (m)	N (/m^2)			DBH (m)	h_v (m)	N (/m^2)		
	0.01	0.40	36			0.10	4.00	0.36		
	Root diameter D_{root} (m)	Root height (m)	Root density N_{root}(/m^2)			Root diameter D_{root} (m)	Root height (m)	Root density N_{root} (/m^2)		
	0.005	0.10	1 008			0.05	1.00	10.08		

[a] DBH is the diameter at the breast height.

still water depths above the artificial platform were varying from 0.3 m to 0.5 m to compare the effects of different submergence volumes of mangrove canopy on wave attenuation. Correspondingly, on the prototype scale, the wave heights range from 0.4 m to 1.6 m, and the wave periods range from 3.16 s to 6.32 s. The scaled and prototype wave conditions are summarized in Table 1.

The wave flume is divided into two sides by a glass wall, and each side is 0.5 m wide. The experiments were carried out and measured on one side of the separated flume. The partition wall is as tall as the side walls of the flume and positioned from the flume end to about two-thirds of this flume from the end. The wave heights on the same cross-sections within the tested region were measured by two wave gauges and found the differences caused by cross-waves were negligible. The diffraction around the partition wall head may affect the local waves around there, but it is sufficiently far from the tested region. In the tested region, we controlled the waves at the G3 position as the incident waves and subtracted the wave height reduction induced by the side wall, the partition wall, and the bottom which were obtained from the bare bottom experiments. Thus, the tested half-flume side can be treated as a separate flume, and the partition wall effects were ignored. The schematic layout of the experiment's apparatus is shown in Fig. 1. The mangrove mimics are displayed in Fig. 2. The artificial mangrove model (AMM) was glutted into a PVC plate, which was drilled into the false flat bottom. In all configurations, the AMM patch was 2.0 m long and 0.5 m wide. The center of the AMM patch was 42 m away from the wave generator. The AMM height is set as 0.4 m high, keeping it constant. The submergence ratio α is defined as the AMM height h_v over the water depth h, changing from emergent ($\alpha > 1$), nearly emergent ($\alpha = 1$) to fully submerged ($\alpha < 1$).

A total of 8 capacitive wave gauges were installed along the centerline of the forest patch to measure the free surface evolution at a 50 Hz sampling frequency. Fig. 1 shows the location of these gauges. Three gauges are located in front of the forest region, of which G3 was placed 1 m in front of the vegetation patch. Five gauges were positioned along the central line of the forest at a distance step of 0.5 m G4 was placed at the leading edge of the vegetation zone. While G8 was placed at the rearing edge of the patch. The reflected waves on the bare bottom by the flume end were separated using the two-point method (Goda and Suzuki, 1976) by G1-G2 far from the tested region. The reflection coefficients were found to be less than 7%. This level of reflection was deemed sufficiently small and would have negligible effects on incident waves (Abdolahpour et al., 2016). All experiments were repeated three times to ensure the repeatability and reliability of the measurements.

3.2. Mangrove model design

The *Rhizophora* sp. is one of the representative types among mangrove species. *Rhizophora* mangroves have been identified as the most distributed around the world (Ohira et al., 2013; Tomiczek et al., 2020b) and as pioneer species directly exposed to wave action (Maza et al., 2021). Such mangrove species have been proven to attenuate wave energy effectively (Massel et al., 1999; Strusínska-Correia et al., 2013; Méndez-Alonzo et al., 2015; Maza et al., 2017). *Rhizophora* sp. has a typical three-layer morphology with conspicuous stilt root (also called prop root), stem, and canopy components. When a major part of a mangrove tree is submerged in a water column, both the submerged roots, stem, and canopy contribute to wave attenuation. As the mangrove morphology is depth-varying, the submergence volume highly depends on the water level. Generally, in previous studies, mangrove forests are simplified as rigid cylinders (Maza et al., 2015; Phan et al., 2019) or parameterized mimics (Ismail et al., 2012; Strusínska-Correia et al., 2013; Maza et al., 2017; Hoque et al., 2018; Wang et al., 2022a). To investigate the wave dynamics within mangrove forests, a proper parametric model to resemble the complex structure of a mangrove tree is important to be selected. In this study, the artificial mangrove model was made on a geometric scale of 1:10, consisting of an

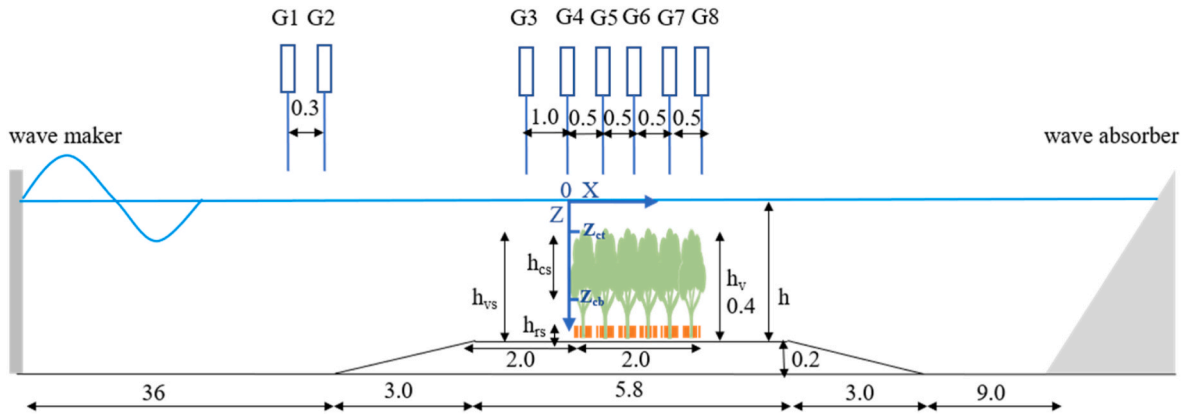

Fig. 1. Sketch of the wave flume setup. G1-G8 denote wave gauges. All dimensions are in meters (not to scale).

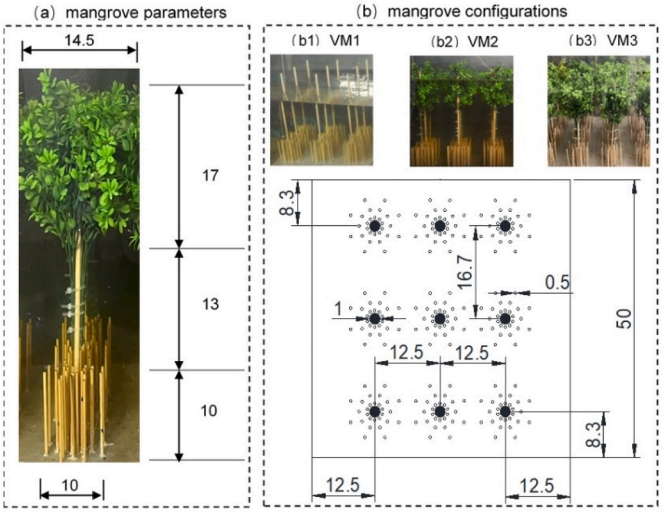

Fig. 2. The artificial mangrove parameters: (a) a single mangrove tree; (b) mangrove patch configuration and layout of model M1, M2, and M3 (units in cm). Not to scale.

entire root, stem, and canopy components. The dimensions of the artificial mangrove mimics are summarized in Table 1. The scaled AMM represented an idealized schematic of the entire mangrove root, stem, and canopy system.

According to a field campaign measuring *Rhizophora apiculata* and *Rhizophora mucronata* trees, Ohira et al. (2013) proposed a morphological model relating typical dimensions of mangroves to the diameter at the breast height (DBH). The sample trees have a 0.03–0.28 m DBH and 6–50 years of age. In this study, a 0.1 m DBH was chosen to design the artificial mangrove mimics, which are between young and mid-age growth stages, referring to Husrin and Oumeraci (2009). The height of the mangrove tree is 4 m based on linear interpolation between the typical parameters of young and mid-age mangroves. Thus, the mangrove model has a 0.4 m height and 0.01 m DBH (Fig. 2). To design the root system, the morphological model proposed by Ohira et al. (2013) was referred to formulate the stilt root shape of the *Rhizophora* sp. with the chosen DBH. The roots of a single mangrove tree were mimicked by 28 wooden rods with a 0.005 m diameter, a 0.1 m height, and a 0.1 m spreading distance. The roots are distributed equally in three concentric circles around the trunk, with a 0.03 m, 0.06 m, and 0.1 m diameter, respectively (Fig. 2). The selected root parameters are similar to the predicted values by the morphology model proposed by Ohira et al. (2013). For instance, the predicted highest root height is 0.126 m, and the root diameter is 0.0034 m. Furthermore, as the morphology model only consider the primary root, we choose a larger root number than the predicted root number. In addition, we ignored the

Table 2
Mangrove model and test configurations.

Mangrove patch configuration	name	components	Stem density (/m^2)	Root density (/m^2)	Canopy density (/m^2)	Leaf area index
	M0	No mangrove	–	–	–	–
	M1	stem + root	36	1 008	–	–
	M2	stem + root +canopy	36	1 008	branch: 252 twig: 1 260 leaf: 18 900	2.42
	M3	stem + root +canopy	36	1 008	branch: 504 twig: 2 520 leaf: 37 800	4.84

Wave conditions	Wave height (m)	Wave periods (s)	Water depth (m)	Mangrove configurations
	0.04	1.0/1.2/1.4	0.3	M0/M1/M3
	0.06	1.2/1.4	0.3	M0/M1/M3
	0.08	1.2/1.4/1.6	0.3	M0/M1/M3
	0.06	1.0/1.2/1.4	0.4	M0/M1/M2/M3
	0.08	1.2/1.4/1.6	0.4	M0/M1/M2/M3
	0.10	1.4/1.6/2.0	0.4	M0/M1/M2/M3
	0.04	1.0	0.5	M0/M1/M2/M3
	0.06	1.2	0.5	M0/M1/M2/M3
	0.08	1.4/1.6/1.8	0.5	M0/M1/M2/M3
	0.12	1.4/1.6/1.8	0.5	M0/M1/M2/M3
	0.16	1.4/1.8/2.0	0.5	M0/M1/M2/M3

interwoven between the roots and assumed the roots as isolated wooden rods with a constant height for simplicity. However, there are limited allometric equations of mangrove canopy attributes. We examined the measured data from literature. Mandal et al. (2019) measured the canopy diameter ranging from 0.1 m to 9 m (mean 2.33 ± 0.24 m) for short *Rhizophora mangle* with a height ranging from 1.4 to 6.2 m (mean 3.9 ± 0.09 m). Domiciano Galvincio and Popescu (2016) compared field data and lidar data, and found the mean canopy diameter was 1.86 m with a mean DBH of 0.12 m of 585 samples. Thus, the canopy having a less than 2 m canopy width would be a reasonable but conservative estimation of mangrove with a 0.10 m DBH. In order to avoid the overlap of neighboring canopies, we choose a 1.45 m canopy width, which is 0.145 m on the small scale. Then, the canopy height was chosen 0.17 m, to be slightly larger than the canopy diameter. Therefore, the canopies were made of polyethylene with a 0.145 m width and a 0.17 m height. To compare with varying complex mangrove canopies, three canopy densities were conducted, representing no canopy, sparse canopy, and dense canopy conditions (Table 2). The canopy model was made of branches and leaves. The breaches have two orders, hereinafter the 1st branch was called branch and the 2nd branch was called twig. The leaves were directly attached to the twigs. To mimic the leaves with nature, we only controlled the leaf area index within a reasonable range, but ignore the single-leaf characteristics of enormous leaves. The leaf area index (LAI) is defined as leaf area per unit horizontal ground surface area (Weiss et al., 2004). In literature, the values of LAI has a wide range which are species specific. Clough and Gong (1997) using the direct measurement obtained the LAI of a 22-year-old *Rhizophora apiculate* stand with a 0.15 m DBH and a 0.30 trees/m^2 density. The measured LAI ranges from 2.2 to 7.4 with a mean value of 4.9. Similarly, the values of LAI of artificial mangrove models in this study were 2.42 for sparse canopy and 4.84 for dense canopy. For the sparse canopy, each canopy consists of 7 branches with a 0.0017 m diameter and a 0.17 m height, and each branch has 5 twigs with a 0.0011 m diameter and a 0.079 m height (Table 1). Each twig has 15 leaves with a 0.0091 m width and 0.018 m length. For the dense canopy, the number of branches, twigs, and leaves doubled that of the sparse canopy, as well as the canopy volume. The volume of each canopy was 5×10^{-5} m^3 of the sparse canopy and 10^{-4} m^3 of the dense canopy. The canopy volume was measured through replacing the water volume by the submerged canopy in a measuring glass cup.

To assess the stiffness of the canopy model, the Cauchy number was compared. The Cauchy number $Ca = (\rho \bar{u}^2 A_p h_v^2)/(E_{ela} I)$, which is defined to express the relative magnitude of hydrodynamic drag and the restoring force due to stiffness (Luhar and Nepf, 2016), where $E_{ela}I$ is the flexural rigidity, E_{ela} [N/m^2] is the elastic modulus, and I [m^4] is the second moment of area. To reach the Cauchy number similar to the prototype, the $\lambda_{E_{ela}}$ should be equal to the geometrical scale λ. The measured elastic modulus of mangrove branches by van Hespen et al. (2021) was between 0.82 and 4 $\times 10^9$ N/m^2, and by Santini et al. (2013) were between 0.50 and 2.3 $\times 10^9$ N/m^2. Thus, the elastic modulus of the mangrove branch model should be the order of magnitude O(10^8) N/m^2. The elastic modulus of the slightly flexible twigs made of polyethylene was measured through the three-point bending test. The length of test twig samples was L_{sample} = 20*d+2 mm, where d is the sample twig diameter, followed by van Hespen et al. (2021). The measured E_{ela} values of 5 twig samples were $4.29 \pm 0.69 \times 10^8$ N/m^2 and its values were within the reasonable range. Given the A_p and h_v of a twig is 8.69 $\times 10^{-5}$ m^2 and 0.079 m respectively (Table 1) and the $\bar{u}$ ranges from 0.061 m/s to 0.32 m/s, the according *Ca* number of the twigs falls within the range of 0.055 and 2.21 on the model scale. The branch model was made of plastic-coated steel wire, which was observed rigid enough to withstand large wave conditions. Therefore, its elastic modulus is not necessary to be concerned. Although the leaves were flexible, their reconfigurations were ignored due to their small size for simplicity and they were assumed functioning as rigid porous barriers. In this study, we only consider the contribution of the dense leaves from the point of increased frontal area.

In the field, such a mangrove with a 0.1 m DBH is about at the age of 15 years old, and the density is approximately 0.337 trees/m^2 (Maza

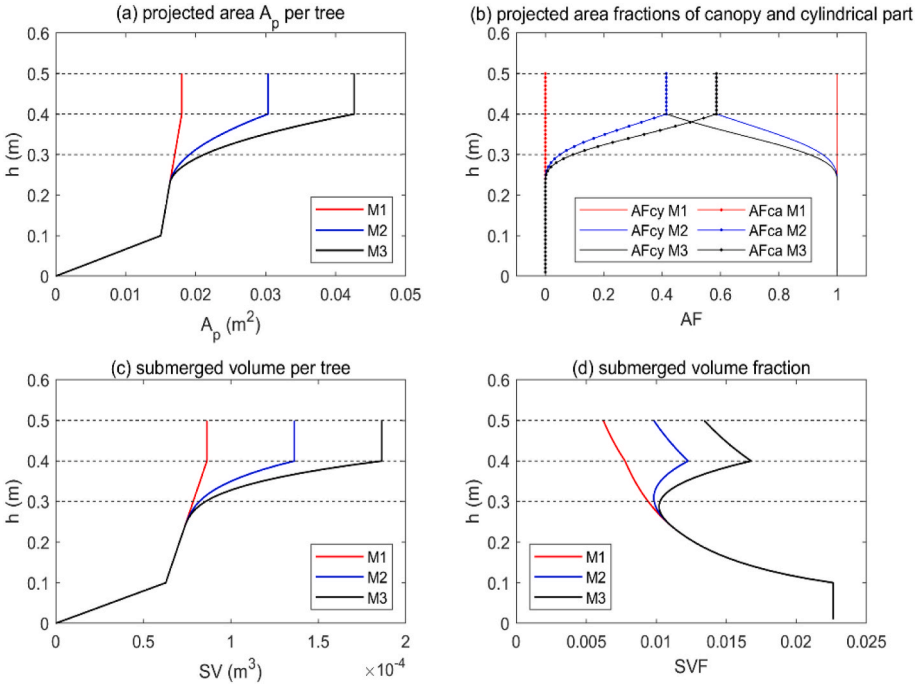

Fig. 3. The vertical variations of the projected area A_p(=Nroot/N*D_{root}*h_{rs} + DBH*h_{vs}+0.5W_{cs}*h_{cs}, where W_{cs} is the maximal width of the submerged canopy, h_{rs} the height of the submerged root); projected area fractions of the canopy AFca(=0.5W_{cs}*h_{cs}/A_p, $AF_{ca,M1}$ = 0, $AF_{ca,M2}$=($A_{p,M2}$-$A_{p,M1}$)/$A_{p,M2}$, $AF_{ca,M3}$=($A_{p,M3}$-$A_{p,M1}$)/$A_{p,M3}$) and cylindrical part including the root and the stem AFcy(=(Nroot/N*D_{root}*h_{rs} + DBH*h_{vs})/A_p, $AF_{cy,M1}$ = 1, $AF_{cy,M2}$ = $A_{p,M1}$/$A_{p,M2}$, $AF_{cy,M3}$ = $A_{p,M1}$/$A_{p,M3}$); submerged volume SV(=N_{root}/N* π*D_{root}^2/4*h_{rs}+ π*DBH^2/4*h_{vs}+(h_{cs}/h_c)^3*V_c); the submerged volume fraction SVF(=N*SV/V, where V=B*W*h, B and W are the length and the width of the mangrove forests, respectively) of the artificial mangrove models.

et al., 2021). Then we set the mangrove density as 0.36 trees/m^2 to fit the wave flume. A total of 36 AMMs were located in the 0.5 m wide and 2 m long forest patch, resulting in a density of 36 trees/m^2 on a model scale or 0.36 trees/m^2 on the prototype scale. In previous studies, the tandem and staggered arrangements of AMMs showed an insignificant difference in wave attenuation (Hashim and Khairuddin, 2014). Thus, the AMMs were arranged only in tandem order in this study (Fig. 2). The distances between each stem are 0.125 m in the transverse direction and 0.167 m in the longitudinal direction, respectively.

The associated submerged volume fractions of varying canopies were based on the water depths (Fig. 3). Assuming the canopy has inverted conoid morphology and the projected area is an inverted triangle, the projected area and submerged volume fractions of the three kinds of mangrove patches are calculated and shown in Fig. 3. With the increasing water depth, the submerged volume fraction (SVF) has a decreasing trend. When the water depth equals to the height of mangrove models M2 and M3, the AMMs are nearly emergent, and the SVF reaches a peak value within the range of 0.3–0.5 m water depth. The length of the mangrove patch is B = 2 m, which ensures fully developed flow within the region when B$\gg A_w$ (Rooijen et al., 2020)., where $A_w = u_m/\omega$ is the wave orbital excursion, and u_m is the peak wave orbital velocity. In addition, the canopy length B is longer than the canopy drag length scale $L_d \sim 2h_v(1-\lambda_p)/\lambda_f$, where λ_f is the frontal area per unit bed area, and λ_p is the plan area per unit bed area (Rooijen et al., 2020). The abovementioned two criteria validate the chosen length of the vegetation zone.

To sum up, 104 tests were carried out with 2 water depths, and 3 different canopy densities of the AMM under 28 wave conditions. For the emergent canopies, 8 wave conditions were tested for M0, M1, and M3. For the nearly emergent canopies, 9 wave conditions were tested for M0-M3. For the fully submerged conditions, 11 wave conditions were tested for M0-M3.

4. Results and discussions

Wave attenuation along the mangrove forest is analyzed in this section. The factors, which affect the wave damping process including the hydrodynamic characteristics and the model characteristics, are

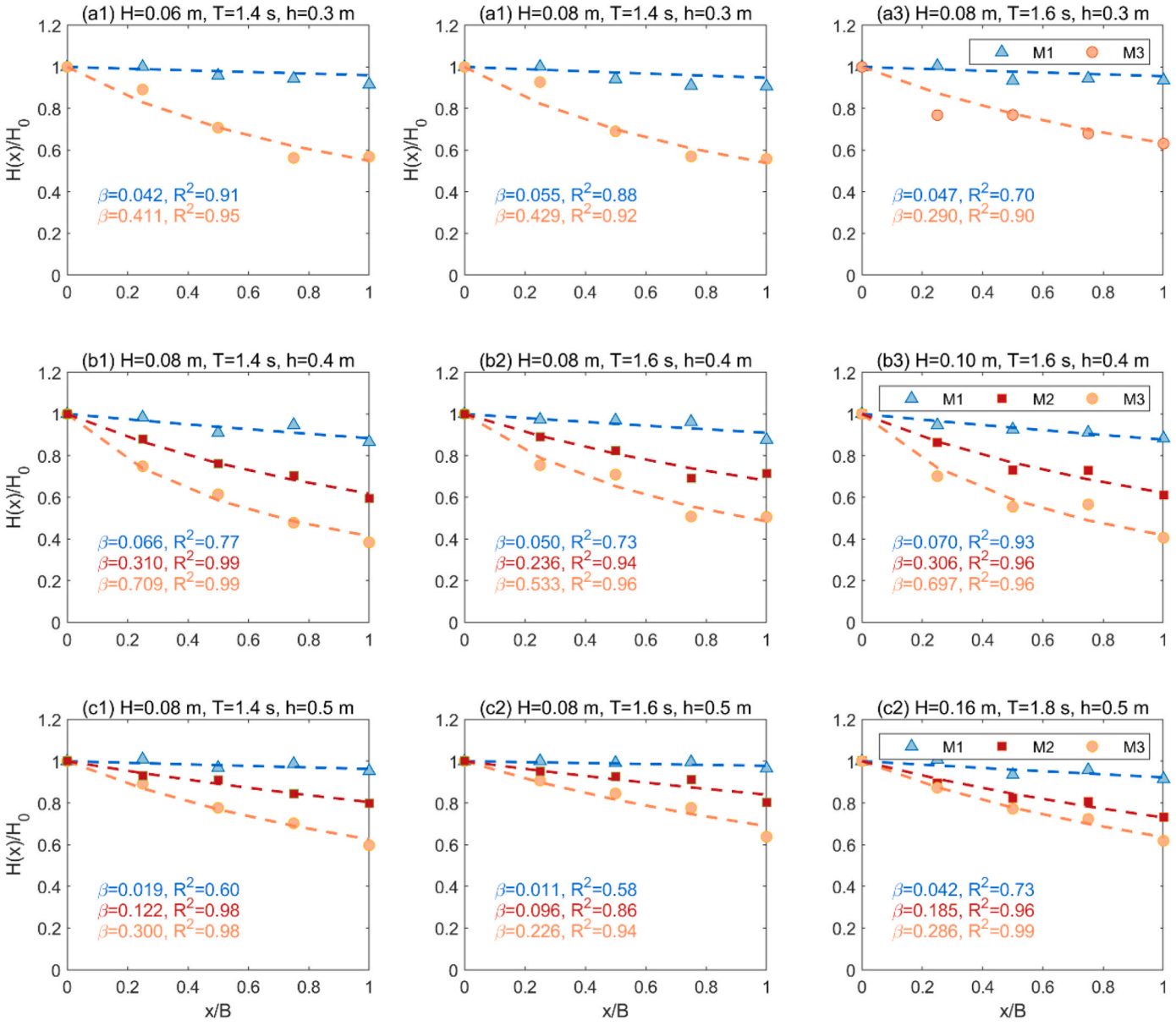

Fig. 4. The wave evolution within three different mangrove patches (blue: M1; red: M2; orange: M3) under representative regular wave conditions. The lines indicated the fitted curve.

compared.

4.1. Wave damping factor β

The wave damping factor β is an essential parameter in quantifying wave attenuation by vegetation. β can be obtained by fitting the measured wave heights along the vegetation patch to Eq. (2), the reduction in wave heights caused by bare bottom and wall friction, which were measured by the controlled experiments without mangrove models (M0) had been subtracted. A larger value of β illustrates a more substantial wave attenuation ability by the vegetation. To compare the differences in contributions by varying canopy densities on wave damping by vegetation (WDV), three mangrove models were designed, including no canopy (M1), small canopy density (M2), and large canopy density (M3). Fig. 4 displays the WDV by the three mangrove models with varying canopy densities (M1, M2, M3) under different hydraulic conditions. The correlation between the relative wave height $H(x)/H_0$ and the wave propagation distance x into the vegetation path was fitted to Eq. (2), employing the nonlinear least squares method. It is shown that when the water depth was 0.3 m and the mangrove models were emergent, although only the lower part of the canopy was submerged ($h_{cs}/h = 0.233$, h_{cs} is the submerged height of canopy), the canopy components contribute substantially to wave attenuation. The corresponding β of the dense canopy model M3 is 7.8 times that of the no-canopy model M1 under the wave climate H = 0.08 m, T = 1.4 s β becomes smaller with the wave period increasing to 1.6 s. Nevertheless, β of the M3 model is 6.2 times that of the M1 model. When the water depth increased to 0.4 m, which is equal to the height of the mangrove models, the relative submerged mangrove canopy height increased to the maximal ($h_{cs}/h = 0.425$), and the damping coefficient increased significantly. β of the M3 model is about 10.7 times that of the M1 model under the presented two wave conditions.

Compared to the M2 model, the canopy volume of the M3 model is two times larger than the M2 model. The consequent β of the M3 model is about two times larger than the M2 model. For the fully submerged condition when the water depth is 0.5 m, the variations of β show a similar trend with the two shallower water depths. However, since the submergence ratio of the canopy decreases ($h_{cs}/h = 0.34$), the damping coefficients β were smallest, less than that under the nearly emergent and the emergent conditions. Therefore, the damping coefficient is dominated by the submerged volume of mangrove forests, especially by the submerged volume fraction of the canopies.

4.2. Key factors affecting wave attenuation

Previous studies show that wave damping is closely related to the mangrove characteristics and the hydrodynamic characteristics (Wu and Cox, 2015; Maza et al., 2019; He et al., 2019; Zhou et al., 2022; Wang et al., 2022b). The relations between the wave damping factor β, the relative water depth *kh,* and the wave steepness *H/L* are shown in Fig. 5. Generally, β increases with the increasing relative water depth *kh* and the wave steepness *H/L* for the same mangrove density and submergence. Fig. 5 shows that when the relative water depth ranges from shallow to deep water, β increases revealing that mangroves attenuate shorter waves more efficiently. β of model M3 is approximately two times the value of model M2, which is consistent with the enhanced two times canopy volumes of the model M3 in comparison to the model M2. Distinctly, the β magnitude of the model M2 and M3 with canopies is one order of magnitude larger than β of model M1 without canopies. This indicates that the canopy component of mangroves can substantially contribute to wave attenuation. The remarkable differences between the cylindrical model M1 and the near-natural model M2 and M3 highlight the importance of quantifying the frontal surface area of woody vegetation (i.e., mangrove trees). Therefore, under inundated deep-water conditions, it is important and necessary to quantify the contribution of submerged canopies to wave attenuation.

Despite the approximately linear trend of β with the relative water depth and wave steepness, the data scatter shown corresponds to a specific model type and wave conditions. Under large water depth h = 0.5 m, big deviation from linear trend of β to large *kh* and *H/L* appeared. To be consistent with the observed wave damping process within the vegetation patch (Figs. 4 and 5), both characteristics of the mangroves and the incident wave conditions were considered by four non-dimensional parameters. The first parameter is the SVF of mangroves which represents the water-blocking volume. It has been reported that the submerged volume of mangroves is a dominant factor that affects wave attenuation (He et al., 2019; Maza et al., 2019). The submerged volume of mangroves depends on the water depth and the variations of mangrove morphology in the vertical direction. Higher submerged volume exerts more drag forces on the water volume and induces stronger wave attenuation. The second parameter is the wave steepness *H/L*. The wave attenuation was observed to increase as wave height increases, but decreases when wave periods (and thus, wavelength) increases (Phan et al., 2014; He et al., 2019). The general trend suggests a positive correlation between β and *H/L* (Maza et al., 2019; Bryant et al.,

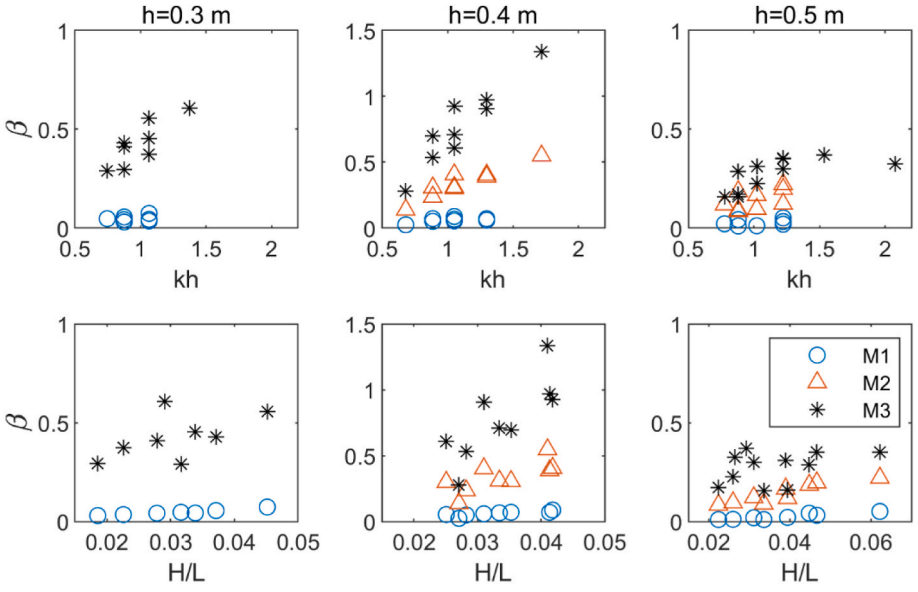

Fig. 5. Variations of the wave damping factor β with relative water depth *kh* and wave steepness *H/L*.

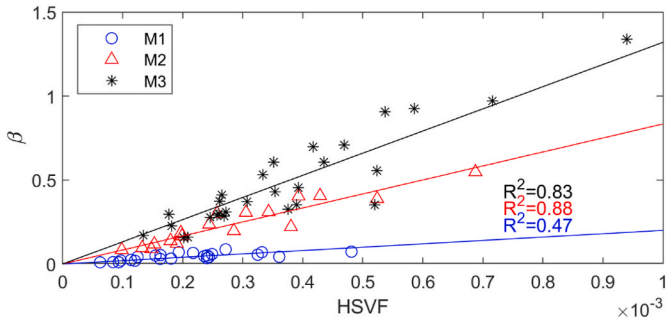

Fig. 6. Wave damping factor β, as a function of the hydraulic submerged volume fraction HSVF under regular wave conditions following the linear fitting relationship of $\beta = \psi \times$ HSVF. The linear fitting lines obtained for three mangrove configurations are displayed respectively (blue: M1; red: M2; black: M3).

2022). The third parameter is the relative forest length, defined as the forest length to the wavelength B/L, considering the effects of wave periods and the importance of the number of wavelengths propagating into the mangrove region. The fourth parameter is the submergence ratio of vegetation, h_{vs}/h, which indicate the effects of varying submerged volume fraction with increasing water depth. Following the definition of the hydraulic standing biomass of saltmarshes (Maza et al., 2022), we defined a new factor in the hydraulic submerged volume fraction HSVF as:

$$\mathrm{HSVF} = \mathrm{SVF} * \frac{H}{L} * \frac{B}{L} * \frac{h_{vs}}{h} \tag{12}$$

In Fig. 6, the relationship between β and the new variable HSVF under regular waves following a linear relationship of $\beta = \psi \times$ HSVF, where ψ was a fitting constant with units of m^{-1}. The linear fitting correlations are expressed as Eqs. (13)–(15), respectively, where values after the addition and subtraction symbol are the standard error of the mean for each coefficient.

$$\text{for M1}: \beta = (199.94 \pm 14.48) * \mathrm{HSVF} \tag{13}$$

$$\text{for M2}: \beta = (833.82 \pm 34.07) * \mathrm{HSVF} \tag{14}$$

$$\text{for M3}: \beta = (1319.90 \pm 54.23) * \mathrm{HSVF} \tag{15}$$

To unify the three correlations of β- HSVF, and separate the contributions of the canopy part and the cylindrical part, i.e. stem and root components, we further defined a variable, the hydraulic submerged volume index (HSVI), by multiplying the HSVF by the submerged volume fraction of canopy part SVFca and the submerged volume fraction of the cylindrical part SVFcy shown in Eq. (16). The c_1 and c_2 coefficients in Eq. (16) were calibrated to obtained the best fit, their values are 1.6 and 1.0, respectively.

$$\mathrm{HSVI} = \mathrm{HSVF} \times (c_1 \times \mathrm{SVFca} + c_2 \times \mathrm{SVFcy}) \tag{16}$$

$$\beta = \left(6.67 \times 10^4 \pm 2.20 \times 10^3\right) * \mathrm{HSVI} \tag{17}$$

In Fig. 7 (a), it is shown that the variations of β of all three models can be well predicted by one HSVI parameter. The fitted correlation between β and HSVI is illustrated by Eq. (17). Fig. 7 (b) depicts the comparison of the predicted wave damping factor β with the measured β. The results show that the empirical relations of β with the HSVI of the sparse canopy model M2 and the dense canopy model M3 fulfill a more confident prediction than the cylindrical model M1. This is because there is a distinct difference between the M2 and M3 models consists of flexible canopies and the M1 models without canopies. Neglecting the introduced uncertainties by mangrove canopy characteristics, the fitting Eq. (17) is a kind of straightforward and efficient way to predict wave damping factor β with simple variables.

To isolate and compare the wave attenuation ability of different mangrove components, we assumed the total wave damping factor β is a linear summation of the wave damping factors of canopy, stem, and root (i.e. β_c, β_s, and β_r respectively) as:

$$\frac{1}{1+\beta x} = \frac{1}{1+\beta_c x} + \frac{1}{1+\beta_s x} + \frac{1}{1+\beta_r x} \tag{18}$$

Each β can be calculated by Equation (4), then the relative wave damping factor of the canopy to stem $\beta_{rc} = \beta_c/\beta_s$ and the relative wave damping factor of root to stem $\beta_{rr} = \beta_r/\beta_s$ were obtained as

$$\beta_{cr} = \frac{\overline{D}_{canopy}\left(\sinh^3(kh_{ct}) + 3\sinh(kh_{ct}) - (\sinh^3(kh_{cb}) + 3\sinh(kh_{cb}))\right)}{\overline{D}_{stem}(\sinh^3(kh_{vs}) + 3\sinh(kh_{vs}))} \tag{19}$$

$$\beta_{rr} = \frac{N_{root}\overline{D}_{root}\left(\sinh^3(kh_{rs}) + 3\sinh(kh_{rs})\right)}{N_{stem}\overline{D}_{stem}(\sinh^3(kh_{vs}) + 3\sinh(kh_{vs}))} \tag{20}$$

where $h_{ct} = h + Z_{ct}$ and $h_{cb} = h + Z_{cb}$, Z_{ct} and $Z_{cb}(= Z_{ct} - h_{cs})$ are the vertical coordinates of the top and bottom of the submerged canopy (see Fig. 1), $\overline{D}_{canopy}$, $\overline{D}_{stem}$ and $\overline{D}_{root}$ is the canopy-depth-averaged, stem-depth-averaged, and root-depth-averaged projected area of canopy, stem, and root respectively.

It is shown in Fig. 8 that β_{rc} increases with increasing kh, but β_{rr} has an opposite decreasing trend with kh. Similarly, a controversy trend between β_{rc} and β_{rr} with Ur existed. β_{rc} decreases with increasing Ur, while β_{rr} increases with increasing Ur. But when Ur is larger than 10, both β_{rc} and β_{rr} are approaching a constant value, which is 3.7 and 1.4 respectively. Accordingly, the contribution of canopy, stem, and root to wave attenuation ability β would be estimated to be 61%, 23%, and 16% respectively.

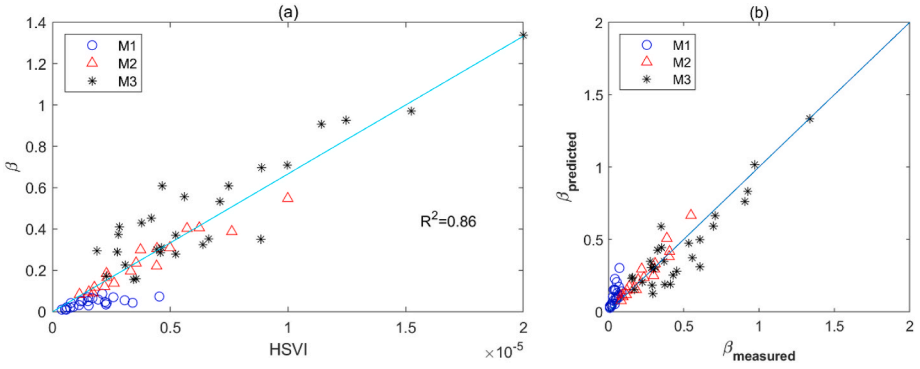

Fig. 7. (a) unified correlation of wave damping factor β and HSVI; (b) comparison between the predicted β by the HSVI and the measured β. The solid line denoted the perfect match line.

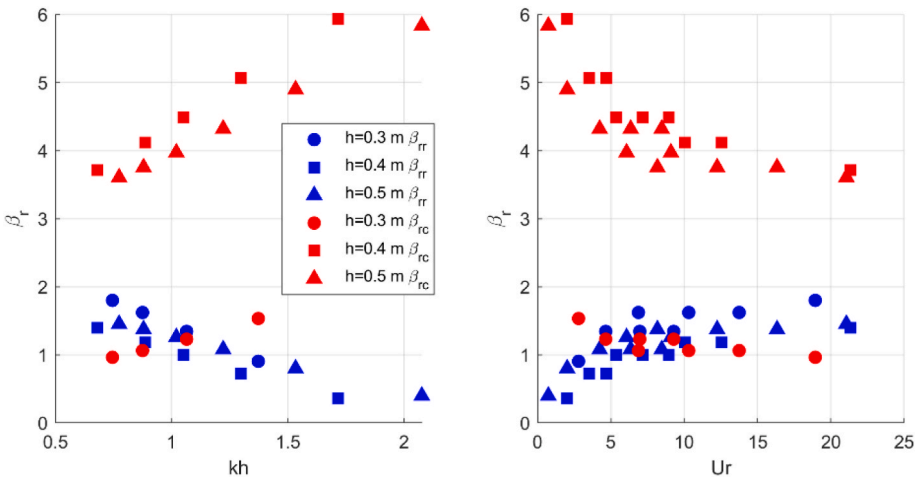

Fig. 8. The variation of relative wave damping factor β_{rc} and β_{rr} with the relative water depth and *Ur* number.

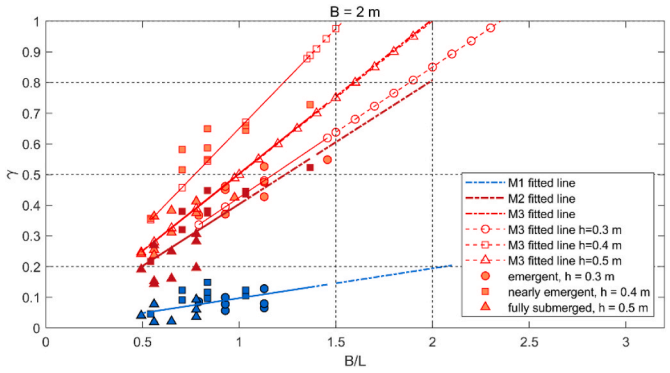

Fig. 9. Variations of the wave height attenuation ratio γ with varying B/L by the three mangrove models under different water depths. The dotted lines denote the average slope of each mangrove model.

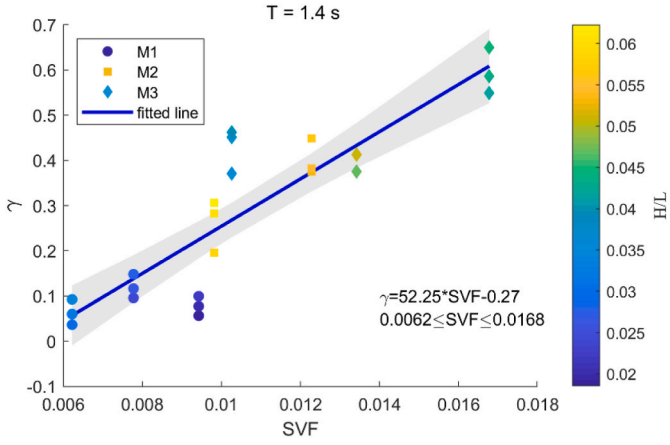

Fig. 10. Variations of the wave height attenuation ratio γ with varying SVF (H = 0.06–0.16 m, T = 1.4 s). The blue line denotes the fitted correlation and the gray zone displays the 95% confidence interval.

It is shown in Fig. 9 that the wave height attenuation ratio $\gamma = 1 - k_t$ induced by the M3 models consisting of dense canopies increases monotonically with the increasing relative vegetation length B/L. While γ has a nonlinear relation with the propagation distance into mangrove forests as k_t, we assumed γ linearly increases with B/L. Under varying water depths, the growth rates of γ with B/L, which are the slopes of the fitted linear lines, are different. Among the emergent, nearly emergent, and fully submerged conditions, the γ growth rate of 0.65 is the largest if the M3 models are nearly emergent, while the smallest is 0.43 if the M3 models are emergent. The average growth rate of γ for M3 is 0.50. It could be predicted that when the width of the mangrove zone equals the incident wavelength, the wave height attenuation ratio γ of model M3 would be 0.5. When B/L is 2. for the M2 model with less dense canopies γ reached 0.8, while for the M1 model without canopies, the γ reduced to 0.2. Such an oversimplified prediction again confirmed the significant contribution of mangrove canopies to wave height attenuation ratio.

In Fig. 9, the approximately linear correlation between the wave height attenuation ratio γ and the relative vegetation width B/L has been elucidated. In addition to the width of the vegetation zone, the effects of the SVF are further compared in Fig. 10, taking tests with wave period T = 1.4 as an example. Undoubtedly, the densest canopy model M3 produced the largest wave height attenuation ratio at about 0.7. Despite the same submerged volume under nearly emergent and fully submerged conditions, the higher SVF under the nearly emergent condition produces a higher wave attenuation. As predicted by the linear fitted line, once the SVF reaches the value of 0.0236, the incident wave energy would be 100% attenuated. It is confirmed again that model M3 of a larger canopy density attenuates wave energy more effectively than model M2 of a smaller canopy density and model M1 of no canopy. Although the canopy is much more flexible than the root and the stem parts, the canopy contributes substantially to wave attenuation ability. It is imperative to account for the canopy contributions when predicting the wave attenuation ability of young mangrove forests because the canopies of young samplings are frequently submerged. Otherwise, only considering the wave attenuation by the root and stem parts, the total wave height attenuation ratio would be significantly underestimated. Therefore, an empirical morphology model of mangroves, including the root, stem, and canopy components, would promote an accurate evaluation of the submerged volume of mangrove forests, and their wave attenuation ability.

4.3. Bulk drag coefficient

According to Eq. (3), the bulk drag coefficient C_D is calculated from the fitted wave damping factor β. The bulk drag coefficient under different wave conditions and different vegetation configurations are compared in Fig. 11. Generally, the correlation between C_D and Re_d, KC_d, or *Ur* presents a similar overall trend to previous studies (Hu et al., 2014, 2022; Wang et al., 2022a). The subscript d represents the characteristic length scale is the DBH. For instance, with the increase of the hydrodynamic characteristic numbers, C_D decreases and gradually approaches a stable minimum value. As shown in Fig. 11, the values of the bulk drag

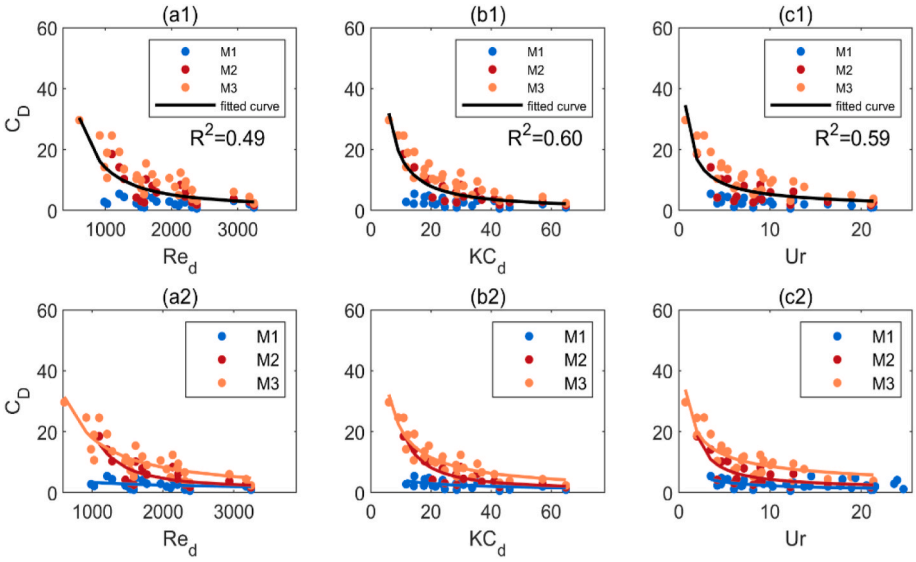

Fig. 11. Variations in C_D with characteristic numbers Re_d, KC_d, or Ur (blue dots: M1; red dots: M2; orange dots: M3). The correlations between the C_D and the characteristic numbers Re_d, KC_d, and Ur are based on the function of $C_D = a_1 + (a_2/\varphi)^{a3}$ in which φ would be Re_d, KC_d, or Ur respectively, a_1, a_2 and a_3 are coefficients. The fitted curves are displayed by solid curves.

coefficient of the artificial mangrove models M2 and M3 with canopies range from 1.78 to 29.7. With increasing Reynolds number, C_D is decreasing. C_D of models M2 and M3 is much larger than that of model M1 without canopies, of which the mean value of C_D is about 2.63. Such a larger C_D value of models with canopies demonstrate the strong ability of the canopy component to attenuate waves, especially under weak wave climates. Similarly, Wu and Cox (2015) demonstrated that C_D is highly dependent on vertical biomass distribution. When the projected area was kept constant, the changes in C_D varies from 140% to 170% between uniform and nonuniform schemes. They highlighted that the assumption of a uniform distribution of vegetation biomass is critical. Therefore, when using the empirical correlations of C_D obtained for cylindrical models to calculate the C_D of mangroves, the complex vertical morphology structure of mangroves should be properly parameterized, especially when the dense canopy part is submerged.

In Fig. 11, the correlations between C_D and the hydraulic parameters Re_d, KC_d, and Ur are compared. Consistent with the findings by Wu and Cox (2015), the bulk drag coefficient can be more accurately predicted by the KC_d and Ur parameters for cylindrical stems than the Re_d number. The respective fitted lines of model M2 and M3 (colored lines in Fig. 11, a2, b2, c2) demonstrated that the two lines would gradually converge when the hydraulic parameters approach their minimum values. However, they are deviating much further from the fitted line of model M1. Therefore, the fitted line of C_D for the total data (black lines in Fig. 11, a1, b1, c1) would significantly overestimate C_D of cylindrical model M1 if the values of hydraulic parameters are small. Wang et al. (2022a) found that the correlation coefficient is higher if the Re is calculated using the hydraulic radius of the vegetation instead of the stem diameter. Comparing the effects of different definitions of Re number by different characteristic length scales, Fig. 12 shows that the R^2 of the fitted Re_{rv}-C_D line significantly increases, while the R^2 of the fitted KC_{rv}-C_D line significantly decreases. Thus, the hydraulic radius of the

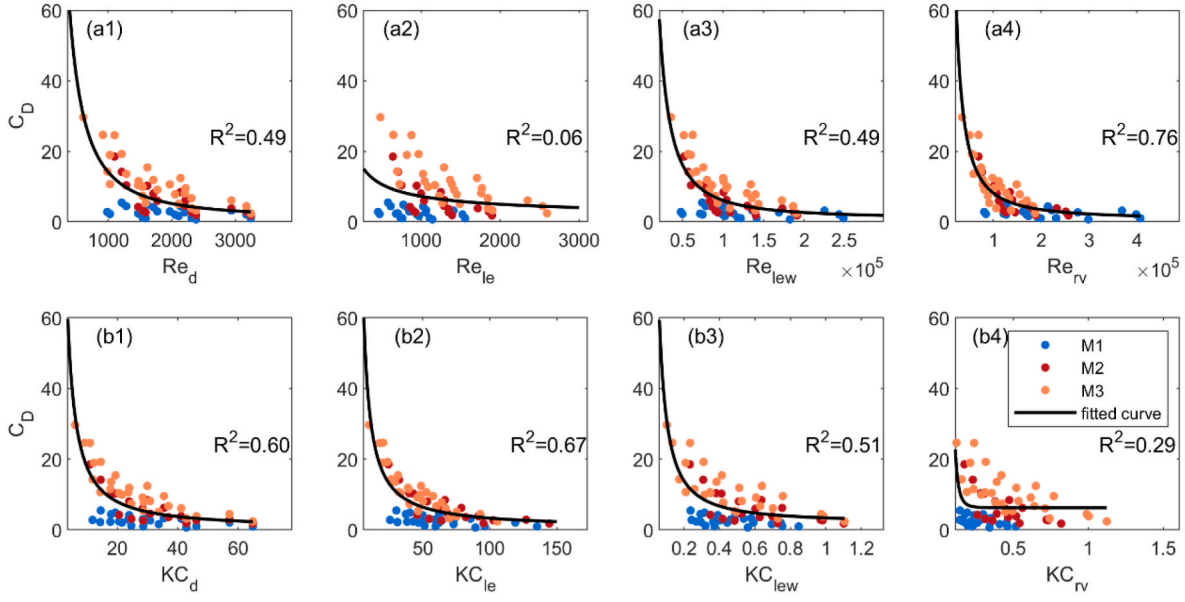

Fig. 12. Correlations of C_D with Re and KC when the length scale is the stem diameter d, effective vegetation length l_e, l_{ew} and hydraulic radius of vegetation r_v, respectively. The blue dots: M1; red dots: M2; orange dots: M3. The solid line denotes the fitted curves.

Table 3
Previously existing and newly proposed empirical formulas of the bulk drag coefficient of mangroves under waves.

Source	Scale 1:λ	Vegetation	Formula	Scope
Maza et al. (2017)	1:12	artificial mangrove with stem, root	$C_D = 9.49 * Re_d^{-0.31}$	$500 < Re_d < 1700$
He et al. (2019)	1:10	artificial mangrove with stem, root, canopy	$C_D = 18.025 * e^{-0.043 KC_d}$	$10 < KC_d < 37$
Wang et al. (2022b)	1:10	artificial mangrove with stem, root	$C_D = 0.42 + \left(\frac{0.77}{KC_{rv}}\right)^{0.41}$	$0.01 < KC_{rv} < 0.28$
Chang et al. (2022)	1:7	artificial mangrove with stem, root	$C_D = 1.15 + \left(\frac{14.70}{KC_d}\right)^{1.065}$	$2.5 < KC_d < 20$
			$C_D = 1.15 + \left(\frac{1015.21}{Re_d}\right)^{1.044}$	$180 < Re_d < 1\,300$
Bryant et al. (2022)	1:2.1	artificial mangrove with stem, root	$C_D = 0.86 + \left(\frac{1.24}{KC_d}\right)^{0.78}$	$0 < KC_d < 12$
Kelty et al. (2022)	1:1	artificial mangrove with stem, root	$C_D = 0.60 + \left(\frac{300000}{Re_d}\right)^{1.0}$	$4\,900 < Re_d < 119\,000$
This study	1:10	artificial mangrove with stem, root, canopy	$C_D = 0.60 + \left(\frac{101.99}{KC_d}\right)^{1.22}$	$6.05 < KC_d < 64.90$
			$C_D = 0.60 + \left(\frac{420000}{Re_{rv}}\right)^{1.41}$	$34\,900 < Re_{rv} < 407\,000$
			$C_D = 0.60 + \left(\frac{80.00}{Ur}\right)^{0.75}$	$0.73 < Ur < 21.33$

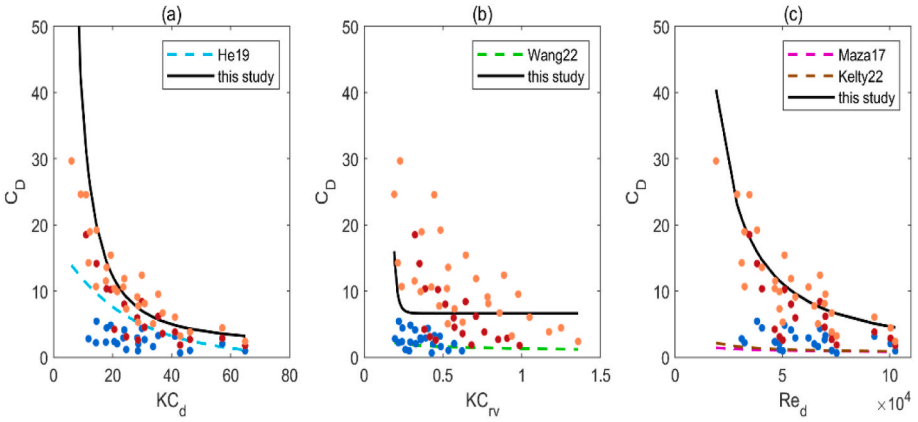

Fig. 13. Comparison with other proposed correlations of C_D with KC_d, KC_{rv} and Re_d (Maza et al., 2017; He et al., 2019; Wang et al., 2022b; Kelty et al., 2022). The Re_d numbers were upscaled to the prototype scale.

vegetation r_v is the best length scale to define Re instead of the stem diameter d, the effective length of vegetation l_e or the effective length scale of water volume l_{ew} for the AMMs. The bulk drag coefficient C_D can be better predicted by the specific Re_{rv} number than the KC_{rv} number, while if only the hydraulic parameters are known, the Ur number is a reliable alternative predictor of C_D. Moreover, the C_D-KC correlation is less sensitive to the length scale than the C_D-Re correlation.

The new proposed correlations of C_D-Re_{rv}, C_D-KC_d for both the cylindrical mangrove model without canopy (M1) and the mangrove model with canopy (M2 and M3) in this study were compared with other available formulas in literature, and all of the formulas were summarized in Table 3. From this study, we presented the C_D-Re_{rv}, C_D-KC_d and C_D-Ur correlations in Table 3 in the form of $C_D = a_1 + (a_2/\varphi)^{a3}$, in which φ would be Re_{rv}, KC_d, or Ur respectively. Following Kelty et al. (2022), the a_1 coefficient was set as 0.6 to be consistent with accepted values of waves on vertical piles. Such a 0.6 value limit the minimum boundary of C_D, and close to the minimum value of C_D obtained in this study which is 0.65. Some formulas are displayed in Fig. 13. It is shown that under larger KC_d conditions, the new formula has a similar curvature of the fitted curve of He et al. (2019). However, when the KC_d is less than 20, the C_D is significantly underestimated by the formula of He et al. (2019). Given the KC_{rv}-C_D correlation, the formula proposed by Wang et al. (2022b) well predicted the C_D for the M1 model with only roots and stems, which is consistent with the mangrove model employed in the experiments by Wang et al. (2022b). This finding also applies to the comparison of C_D-Re_d correlation between Maza et al. (2017) and this study, as Maza et al. (2017) also only focus on the lower part of mangroves consisting of bottom roots and stems. Through the above-mentioned comparison, it can be concluded that it should be careful to use previously existing formulas to predict the C_D of mangroves while the submergence conditions of canopies are different. Otherwise, the formulas deduced for cylindrical models by Maza et al. (2017) and Wang et al. (2022b) would underestimate C_D once mangrove canopies are submerged.

In Fig. 13, the deviations between C_D of cylindrical mangroves without canopies (Maza et al., 2013; Wang et al., 2022b) and mangroves with canopies (this study and He et al., 2019) are significant. In Fig. 14, only the C_D of cylindrical models was compared. The deviations are within an acceptable range. Thus, when applying the empirical models of C_D, not only the hydraulic dynamics should be within their application ranges, but also the characteristics of vegetation should be similar. However, using the C_D of cylindrical models to predict the C_D of mangroves with submerged canopies can be the most conservative prediction.

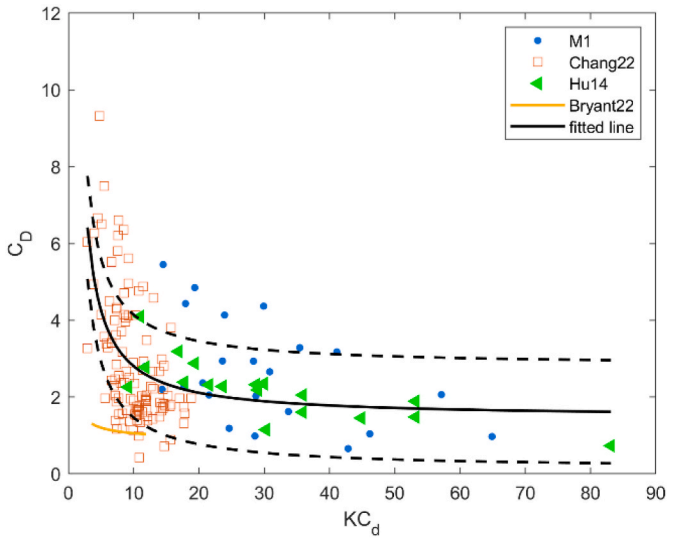

Fig. 14. Comparison with other proposed formulas of C_D-KC_d for cylindrical vegetation with the M1 model (Hu et al., 2014; Chang et al., 2022; Bryant et al., 2022).

4.4. The scaling effects

In literature, a lot of empirical equations have been obtained from small scaled laboratory experiments. Through prototype scale experiments, Kelty et al. (2022) raised attention to the scaling effects of the Reynolds number, when comparing different empirical equations of C_D. This is because the kinetic viscosity in the Reynolds number were usually not scaled down in small scaled laboratory experiments and raised above-mentioned scale effects. It is necessary to rescale Re to the same scale, i.e. the prototype scale, by multiplying $\lambda^{3/2}$, where λ is the geometric scale of the prototype to model. Otherwise, the calculated C_D would deviate from the correct values (Fig. 15, a). To address this scaling issue between different formulas, the prototype $Re_{d,prototype}$ is firstly descaled to $Re_{d,scaled}$ on the same scale as the experiments from which the empirical formulas were induced, then the C_D were calculated by the accordingly empirical formulas, and a new C_D-$Re_{d,prototype}$ correlation was obtained. In this way, it is shown that the C_D-$Re_{d,prototype}$ can fall within a reasonable range (Fig. 15, b). Thus, the correlations between the predicted C_D by different equations obtained on varying scales (1:12 by Maza et al., 2017, 1:10 by this study; 1:7 by Chang et al., 2022, 1:2.1 by Bryant et al., 2022, 1:1 by Kelty et al., 2022), and the corresponding $Re_{d,prototype}$ on the same prototype scale show a fair agreement with each other. However, the KC and Ur numbers are properly scaled according to Froud similarity in models, unlike the Re number. Finding the best parameters from the best fitting performance of empirical formulas obtained from scaled experiments is still a challenging thing, because not a single parameter incorporates all the physical processes. Moreover, valid data from experiments on the prototype scale are still rare and in urgent demand.

5. Conclusions

An experimental study was carried out using a 1:10 artificial mangrove model patch of 2 m width consisting of 36 artificial mangrove models to mimic short mangroves with the root, stem, and canopy components. Regular waves are scaled down using Froude similarity to represent the coastal hydrodynamics. The hydraulic conditions spanned a wave steepness H/L from 0.0186 to 0.0622, and a relative water depth from near shallow to near deep water waves ($0.68 \leq kh \leq 2.08$). The relative wave height ranged in $0.08 \leq H/h \leq 0.32$. The influences of different water depths are tested to investigate the submerged volume fractions of the mangroves under emergent, nearly emergent, and fully submerged conditions. This study gives a new insight into wave attenuation by mangrove morphology structures, focusing on the attribution from the submerged canopy parts. Three canopy densities of mangroves (i.e. no canopy, sparse canopy, and dense canopy) are tested to quantify the wave attenuation contributed by the submerged canopies. The free surface waves propagating into the mangrove forests were measured along the centerline of the patch and analyzed.

The equations proposed by Dalrymple et al. (1984), relating the wave damping factor and the drag coefficient, are employed to calculate the C_D coefficients. A new variable hydraulic submerged volume index ($HSVI$) was defined to predict the wave damping factor β by the mangroves based on the fitted linear correlation. The correlation between the C_D and vegetation characteristic numbers (i.e., the relative width of the patch B/L, or the submerged volume fraction SVF) and the hydrodynamic characteristic numbers (i.e., Reynolds number Re, Keulegan–Carpenter number KC, and Ursell number Ur). The Ursell number was in the range of $0.73 \leq Ur \leq 21.33$. Choosing the stem diameter as the characteristic length scale, the KC number was in the range of $12.97 \leq$

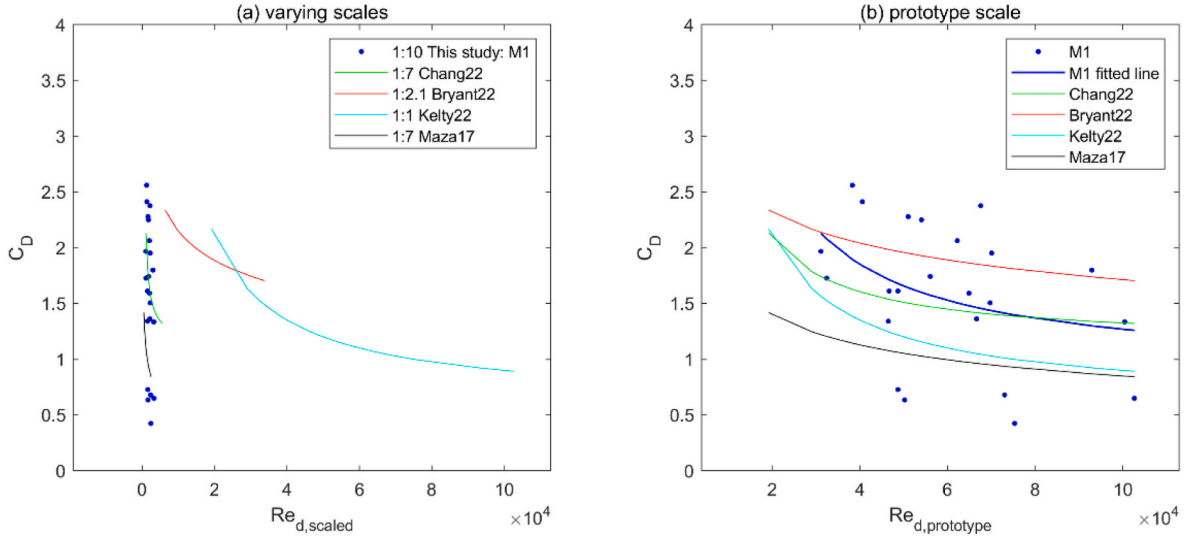

Fig. 15. Comparison with other proposed formulas of C_D-Re on different scales (a) and on prototype scale (b), (Maza et al., 2017; Kelty et al., 2022; Chang et al., 2022; Bryant et al., 2022).

$KC_d \leq 77.39$, and the range of Reynolds number Re_d was between 1.28×10^3 and 4.27×10^3. The analyses show that the correlation of C_D with hydrodynamic characteristic numbers *Re*, *KC,* and *Ur* depends on the characteristic length scale. Among them, the specific C_D-Re_{rv} correlation predicts the best with the highest correlation coefficient. While the C_D-*Re* and C_D-*KC* correlations are highly characteristic length scale dependent, the *Ur* is a reliable predictor of C_D with fair confidence when only the hydraulic parameters are known. Moreover, C_D-*KC* and C_D-*Ur* correlations don't need to consider the scaling effects. However, given the *Re* number, only if the *Re* number were rescaled to compensate the scaling effects raised by the non-scaled kinetic viscosity on small scale, new C_D-*Re* correlations on the prototype scale do have similar trends and show a reasonable agreement with each other.

This study highlights that the canopies of short mangroves (e.g., short species or young saplings) significantly contribute to wave damping once the canopies are submerged. Otherwise, if the canopy effects are not considered, the wave attenuation ability of submerged short mangrove forests would be significantly underestimated. The obtained empirical wave attenuation formula considering the wave decay produced by the canopies is essential to evaluate the wave attenuation performance when short mangrove forests are inundated. For instance, under storm surges, when the water depth increases heavily, the canopies are likely to be submerged and contribute to wave decay. The empirical formula is an excellent supplement to previous studies, highlighting canopy effects on wave attenuation. Incorporating the canopy effects in evaluating wave attenuation ability by mangrove forests would increase the accuracy, but ignoring the canopy effects is still the most conservative way at least. In this study, the effects of biomechanical characteristics of canopy branches and leaves on wave attenuation were ignored, which is worthy of further investigation. Under strong wind and waves, the defoliation of leaves, breakage of branches, and movement of the canopies would need to be carefully considered in future research. The further improvement of prediction would then benefit and facilitate the design and management of a mangrove restoration project.

CRediT authorship contribution statement

Rong Zhang: Conceptualization, Methodology, Investigation, Formal analysis, Visualization, Writing – original draft, preparation. **Yongping Chen:** Supervision, Writing – review & editing. **Jiaxin Lei:** Investigation. **Xin Zhou:** Writing – review & editing. **Peng Yao:** Investigation, Validation, Writing – review & editing. **Marcel J.F. Stive:** Supervision, Writing – review & editing.

Declaration of competing interest

The authors declare that they have no known competing financial interests or personal relationships that could have appeared to influence the work reported in this paper.

Data availability

Data will be made available on request.

Acknowledgments

The laboratory work was assisted by Yuan Wang and Jinya Mei. This work was sponsored by grants from the State Environmental Protection Key Laboratory of Marine Ecosystem Restoration (2023-09), the Fundamental Research Funds for the Central Universities of China (B220202078), the Scientific Research Fund of the Second Institute of Oceanography, Ministry of Natural Resources, China (JG1801), the National Natural Science Foundation of China (52201320), the International Postdoctoral Exchange Fellowship Program of China (YJ20210073).

References

Abdolahpour, M., Ghisalberti, M., Lavery, P., McMahon, K., 2016. Vertical mixing in coastal canopies. Limnol. Oceanogr. 62, 26–42. https://doi.org/10.1002/lno.10368.

Alongi, D.M., 2008. Mangrove forests: resilience, protection from tsunamis, and responses to global climate change. Estuar. Coast Shelf Sci. 76, 1–13. https://doi.org/10.1016/j.ecss.2007.08.024.

Alongi, D.M., 2002. Present state and future of the world's mangrove forests. Environ. Conserv. 29, 331–349.

Anderson, M.E., Smith, J.M., 2014. Wave attenuation by flexible, idealized salt marsh vegetation. Coast. Eng. 83, 82–92. https://doi.org/10.1016/j.coastaleng.2013.10.004.

Barbier, E.B., 2006. Natural barriers to natural disasters: replanting mangroves after the tsunami. Front. Ecol. Environ. 4, 124–131. https://doi.org/10.1890/1540-9295(2006)004[0124:NBTNDR]2.0.CO;2.

Borsje, B.W., van Wesenbeeck, B.K., Dekker, F., Paalvast, P., Bouma, T.J., van Katwijk, M.M., de Vries, M.B., 2011. How ecological engineering can serve in coastal protection. Ecol. Eng. https://doi.org/10.1016/j.ecoleng.2010.11.027.

Brinkman, R.M., 2006. Wave Attenuation in Mangrove Forests: an Investigation through Field and Theoretical Studies. James Cook University.

Bryant, M.A., Bryant, D.B., Provost, L.A., Hurst, N., Mchugh, M., Wargula, A., Tomiczek, T., 2022. Wave Attenuation of Coastal Mangroves at a Near-Prototype Scale. Washington.

Chang, C.-W., Mori, N., Tsuruta, N., Suzuki, K., 2022. An experimental study of mangrove-induced resistance on water waves considering the impacts of typical Rhizophora roots. J. Geophys. Res. Ocean. 1–23. https://doi.org/10.1029/2022JC018653.

Chang, C.-W., Mori, N., Tsuruta, N., Suzuki, K., 2019. Estimation of wave force coefficients on mangrove models. J. Japan Soc. Civ. Eng. Ser. B2 (Coastal Eng. 75 https://doi.org/10.2208/kaigan.75.i_1105. I_1105-I_1110.

Chang, C., Mori, N., 2021. Green infrastructure for the reduction of coastal disasters : a review of the protective role of coastal forests against tsunami, storm surge, and wind waves. Coast Eng. J. 63, 370–385. https://doi.org/10.1080/21664250.2021.1929742.

Cheng, N.-S., Nguyen, H.T., 2011. Hydraulic radius for evaluating resistance induced by simulated emergent vegetation in open-channel flows. J. Hydraul. Eng. 137, 995–1004. https://doi.org/10.1061/(ASCE)HY.1943-7900.

Clough, B.F., Gong, J.E.O.W.K., 1997. Estimating leaf area index and photosynthe production in canopies of the mangrove. Rhizophora apiculata 159, 285–292.

Dahdouh-Guebas, F., Jayatissa, L.P., Nitto, D. Di, Bosire, J.O., Seen, D. Lo, Koedam, N., 2013. How effective were mangroves as a defence against the recent tsunami? Curr. Biol. 15, 443–447. https://doi.org/10.2307/2387877.

Dalrymple, R.A., Kirby, J.T., Hwang, P.A., 1984. Wave diffraction due to areas of energy dissipation. J. Waterw. Port, Coast. Ocean Eng. 110, 67–79.

Danielsen, F., Sørensen, M.K., Olwig, M.F., Selvam, V., Parish, F., Burgess, N.D., Hiraishi, T., Karunagaran, V.M., Rasmussen, M.S., Hansen, L.B., Quarto, A., Suryadiputra, N., 2005. The Asian tsunami: a protective role for coastal vegetation. Science 310, 643. https://doi.org/10.1126/science.1118387.

Das, S., Vincent, J.R., 2009. Mangroves protected villages and reduced death toll during Indian super cyclone. Proc. Natl. Acad. Sci. U.S.A. 106, 7357–7360. https://doi.org/10.1073/pnas.0810440106.

Domiciano Galvincio, J., Popescu, S.C., 2016. Measuring individual tree height and crown diameter for mangrove trees with airborne lidar data. Int. J. Adv. Eng. Manag. Sci. Infogain Publ. (Infogainpublication.com 2, 2454–1311.

Feagin, R.A., Mukherjee, N., Shanker, K., Baird, A.H., Cinner, J., Kerr, A.M., Koedam, N., Sridhar, A., Arthur, R., Jayatissa, L.P., Lo Seen, D., Menon, M., Rodriguez, S., Shamsuddoha, M., Dahdouh-Guebas, F., 2010. Shelter from the storm? Use and misuse of coastal vegetation bioshields for managing natural disasters. Conserv. Lett. 3, 1–11. https://doi.org/10.1111/j.1755-263X.2009.00087.x.

Gedan, K.B., Kirwan, M.L., Wolanski, E., Barbier, E.B., Silliman, B.R., 2011. The present and future role of coastal wetland vegetation in protecting shorelines: answering recent challenges to the paradigm. Clim. Change 106, 7–29. https://doi.org/10.1007/s10584-010-0003-7.

Gijsman, R., Horstman, E.M., Wal, D. Van Der, Friess, D.A., 2021. Nature-Based Engineering : A Review on Reducing Coastal Flood Risk with Mangroves, vol. 8. https://doi.org/10.3389/fmars.2021.702412.

Goda, Y., Suzuki, Y., 1976. Estimation of incident and reflected waves in regular wave experiments. In: Coastal Engineering Proceedings, pp. 828–845. https://doi.org/10.1016/0029-8018(93)E0011-G.

Hadi, S., Latief Muliddin., H., 2003. Analysis of surface wave attenuation in mangrove forests. ITB J. Eng. Sci. 35, 89–108. https://doi.org/10.5614/itbj.eng.sci.2003.35.2.1.

Hashim, A.M., Catherine, S.M.P., Takaijudin, H., 2013. Effectiveness of mangrove forests in surface wave attenuation: a review. Res. J. Appl. Sci. Eng. Technol. 5, 4483–4488. https://doi.org/10.19026/rjaset.5.4361.

Hashim, A.M., Khairuddin, N., 2014. Performance of mangrove forests in coastal protection. Appl. Mech. Mater. 567, 277–282. https://doi.org/10.4028/www.scientific.net/AMM.567.277.

He, F., Chen, J., Jiang, C., 2019. Surface wave attenuation by vegetation with the stem, root and canopy. Coast. Eng. 152, 103509 https://doi.org/10.1016/j.coastaleng.2019.103509.

Hespen, R. Van, Hu, Z., Borsje, B., Dominicis, M. De, Friess, D.A., Stocken, T. Van Der, Wesenbeeck, B. Van, Xie, D., Bouma, T.J., 2023. Mangrove forests as a nature-based solution for coastal flood protection : biophysical and ecological considerations. Water Sci. Eng. 16, 1–13. https://doi.org/10.1016/j.wse.2022.10.004.

Hoque, A., Husrin, S., Oumeraci, H., 2018. Laboratory studies of wave attenuation by coastal forest under storm surge. Coast Eng. J. 60, 225–238. https://doi.org/10.1080/21664250.2018.1486268.
Horstman, E.M., Dohmen-Janssen, C.M., Narra, P.M.F., van den Berg, N.J.F., Siemerink, M., Hulscher, S.J.M.H., 2014. Wave attenuation in mangroves: a quantitative approach to field observations. Coast. Eng. 94, 47–62. https://doi.org/10.1016/j.coastaleng.2014.08.005.
Hu, Z., Lian, S., Zitman, T., Wang, H., He, Z., Wei, H., Ren, L., Uijttewaal, W., Suzuki, T., 2022. Wave breaking induced by opposing currents in submerged vegetation canopies. Water Resour. Res. 58, 1–19. https://doi.org/10.1029/2021WR031121.
Hu, Z., Suzuki, T., Zitman, T., Uittewaal, W., Stive, M., 2014. Laboratory study on wave dissipation by vegetation in combined current – wave flow. Coast. Eng. 88, 131–142.
Husrin, S., Oumeraci, H., 2009. Parameterization of coastal forest vegetation and hydraulic resistance coefficients for tsunami modelling. 4th Annu. Int. Work. Expo Sumatra Tsunami Disaster Recover 78–86.
Ismail, H., Abd Wahab, A.K., Alias, N.E., 2012. Determination of mangrove forest performance in reducing tsunami run-up using physical models. Nat. Hazards 63, 939–963. https://doi.org/10.1007/s11069-012-0200-y.
Kelty, K., Tomiczek, T., Cox, D.T., Lomonaco, P., Mitchell, W., 2022. Prototype-scale physical model of wave attenuation through a mangrove forest of moderate cross-shore thickness: LiDAR-based characterization and Reynolds scaling for engineering with nature. Front. Mar. Sci. 8, 1–18. https://doi.org/10.3389/fmars.2021.780946.
Lee, W.K., Tay, S.H.X., Ooi, S.K., Friess, D.A., 2021. Potential short wave attenuation function of disturbed mangroves. Estuar. Coast Shelf Sci. 248, 106747 https://doi.org/10.1016/j.ecss.2020.106747.
Lou, S., Chen, M., Ma, G., Liu, S., Zhong, G., 2018. Laboratory study of the effect of vertically varying vegetation density on waves, currents and wave-current interactions. Appl. Ocean Res. 79, 74–87. https://doi.org/10.1016/j.apor.2018.07.012.
Luhar, M., Nepf, H.M., 2016. Wave-induced dynamics of flexible blades. J. Fluid Struct. 61, 20–41. https://doi.org/10.1016/j.jfluidstructs.2015.11.007.
Mandal, A., Smith, R.A., Edwards, T., Kinlocke, R., Mitchell, S., Webber, M., Trench, C., Francis, P., Spence, A., 2019. Forces of nature. Local Scale Assessments on Mangrove Ecosystems Status and their Role in Coastal Resilience (Chapter 4):
Massel, S.R., Furukawa, K., Brinkman, R.M., 1999. Surface wave propagation in mangrove forests. Fluid Dynam. Res. 24, 219–249. https://doi.org/10.1016/S0169-5983(98)00024-0.
Maza, M., Adler, K., Ramos, D., Garcia, A.M., Nepf, H., 2017. Velocity and drag evolution from the leading edge of a model mangrove forest. J. Geophys. Res. Ocean. 122, 9144–9159. https://doi.org/10.1002/2017JC012945.
Maza, M., Lara, J.L., Losada, I.J., 2022. A paradigm shift in the quantification of wave energy attenuation due to saltmarshes based on their standing biomass. Sci. Rep. 1–13. https://doi.org/10.1038/s41598-022-18143-6.
Maza, M., Lara, J.L., Losada, I.J., 2019. Experimental analysis of wave attenuation and drag forces in a realistic fringe Rhizophora mangrove forest. Adv. Water Resour. 131, 103376 https://doi.org/10.1016/j.advwatres.2019.07.006.
Maza, M., Lara, J.L., Losada, I.J., 2015. Tsunami wave interaction with mangrove forests: a 3-D numerical approach. Coast. Eng. 98, 33–54. https://doi.org/10.1016/j.coastaleng.2015.01.002.
Maza, M., Lara, J.L., Losada, I.J., 2013. A coupled model of submerged vegetation under oscillatory flow using Navier-Stokes equations. Coast. Eng. 80, 16–34. https://doi.org/10.1016/j.coastaleng.2013.04.009.
Maza, M., Lara, J.L., Losada, J., 2021. Predicting the evolution of coastal protection service with mangrove forest age. Coast. Eng. 168, 103922 https://doi.org/10.1016/j.coastaleng.2021.103922.
Mazda, Y., 1997. Mangroves as a coastal protection from waves in Tong King delta, Vietnam. Mangroves Salt Marshes 127–135.
Mazda, Y., Magi, M., Ikeda, Y., Kurokawa, T., Asano, T., 2006. Wave reduction in a mangrove forest dominated by Sonneratia sp. Wetl. Ecol. Manag. 14, 365–378. https://doi.org/10.1007/s11273-005-5388-0.
Mazda, Y., Wolanski, E., King, B., Sase, A., Ohtsuka, D., Magi, M., 1997. Drag force due to vegetation in mangrove swamps. Mangroves Salt Marshes 1, 193–199. https://doi.org/10.1023/A:1009949411068.
Méndez-Alonzo, R., Moctezuma, C., Ordoñez, V.R., Angeles, G., Martínez, A.J., López-Portillo, J., 2015. Root biomechanics in Rhizophora mangle: anatomy, morphology and ecology of mangrove's flying buttresses. Ann. Bot. 115, 833–840. https://doi.org/10.1093/aob/mcv002.
Mendez, F.J., Losada, I.J., Losada, M.A., 1999. Hydrodynamics induced by wind waves in a vegetation field. J. Geophys. Res. 104, 18383–18396.
Menéndez, P., Losada, I.J., Torres-Ortega, S., Narayan, S., Beck, M.W., 2020. The global flood protection benefits of mangroves. Sci. Rep. 10, 4404. https://doi.org/10.1038/s41598-020-61136-6.
Mullarney, J.C., Henderson, S.M., Reyns, J.A.H., Norris, B.K., Bryan, K.R., 2017. Spatially varying drag within a wave-exposed mangrove forest and on the adjacent tidal flat. Continent. Shelf Res. 147, 102–113. https://doi.org/10.1016/j.csr.2017.06.019.
Ohira, W., Honda, K., Nagai, M., Ratanasuwan, A., 2013. Mangrove stilt root morphology modeling for estimating hydraulic drag in tsunami inundation simulation. Trees Struct. Funct. 27, 141–148. https://doi.org/10.1007/s00468-012-0782-8.
Osorio, A., Piedrahita, A., Arredondo, M., Osorio-Cano, J., Henao, A., Cáceres-Euse, A., Urrego, L., Delgado, J., 2019. Study of the velocity and wave damping in a physical model of a mangrove forest including secondary roots. In: Coastal Structures 2019, pp. 1055–1064. https://doi.org/10.18451/978-3-939230-64-9. Hannover.
Othman, M.A., 1994. Value of mangroves in coastal protection. Hydrobiologia 285, 277–282. https://doi.org/10.1007/BF00005674.
Pan, Y., Yin, S., Chen, Y.P., Yang, Y.B., Xu, C.Y., Xu, Z.S., 2022. An experimental study on the evolution of a submerged berm under the effects of regular waves in low-energy conditions. Coast. Eng. 176 https://doi.org/10.1016/j.coastaleng.2022.104169.
Pan, Y., Zhou, Z.J., Chen, Y.P., 2020. An analysis of the downward-flushing flow on the crest of a levee under combined wave and surge overtopping. Coast. Eng. 158, 103701 https://doi.org/10.1016/j.coastaleng.2020.103701.
Phan, K.L., Stive, M.J.F., Zijlema, M., Truong, H.S., Aarninkhof, S.G.J., 2019. The effects of wave non-linearity on wave attenuation by vegetation. Coast. Eng. 147, 63–74. https://doi.org/10.1016/j.coastaleng.2019.01.004.
Phan, L.K., van Thiel de Vries, J.S.M., Stive, M.J.F., 2014. Coastal mangrove squeeze in the mekong delta. J. Coast Res. 300, 233–243. https://doi.org/10.2112/jcoastres-d-14-00049.1.
Rooijen, A., Lowe, R., Rijnsdorp, D.P., Ghisalberti, M., Jacobsen, N.G., McCall, R., 2020. Wave-driven mean flow dynamics in submerged canopies. J. Geophys. Res. Ocean. 125 https://doi.org/10.1029/2019JC015935.
Saenger, P., 2002. Mangrove Ecology, Silviculture and Conservation. https://doi.org/10.1007/978-94-015-9962-7.
Santini, N.S., Schmitz, N., Bennion, V., Lovelock, C.E., 2013. The anatomical basis of the link between density and mechanical strength in mangrove branches. Funct. Plant Biol. 40, 400–408. https://doi.org/10.1071/FP12204.
Schoonees, T., Gijón Mancheño, A., Scheres, B., Bouma, T.J., Silva, R., Schlurmann, T., Schüttrumpf, H., 2019. Hard structures for coastal protection, towards greener designs. Estuar. Coast 42, 1709–1729. https://doi.org/10.1007/s12237-019-00551-z.
Spalding, M.D., Ruffo, S., Lacambra, C., Meliane, I., Hale, L.Z., Shepard, C.C., Beck, M.W., 2014. The role of ecosystems in coastal protection: adapting to climate change and coastal hazards. Ocean Coast Manag. 90, 50–57. https://doi.org/10.1016/j.ocecoaman.2013.09.007.
Strusínska-Correia, A., Husrin, S., Oumeraci, H., 2013. Tsunami damping by mangrove forest: a laboratory study using parameterized trees. Nat. Hazards Earth Syst. Sci. 13, 483–503. https://doi.org/10.5194/nhess-13-483-2013.
Suzuki, T., Hu, Z., Kumada, K., Phan, L.K., Zijlema, M., 2019. Non-hydrostatic modeling of drag, inertia and porous effects in wave propagation over dense vegetation fields. Coast. Eng. 149, 49–64. https://doi.org/10.1016/j.coastaleng.2019.03.011.
Tanaka, N., Sasaki, Y., Mowjood, M.I.M., Jinadasa, K.B.S.N., Homchuen, S., 2007. Coastal vegetation structures and their functions in tsunami protection: experience of the recent Indian Ocean tsunami. Landsc. Ecol. Eng. 3, 33–45. https://doi.org/10.1007/s11355-006-0013-9.
Tang, J., Shen, S., Wang, H., 2015. Numerical model for coastal wave propagation through mild slope zone in the presence of rigid vegetation. Coast. Eng. 97, 53–59. https://doi.org/10.1016/j.coastaleng.2014.12.006.
Tang, J., Shen, Y., Causon, D.M., Qian, L., Mingham, C.G., 2017. Numerical study of periodic long wave run-up on a rigid vegetation sloping beach. Coast. Eng. 121, 158–166. https://doi.org/10.1016/j.coastaleng.2016.12.004.
Tang, J., Zhao, C., Shen, Y., 2019. Numerical investigation of the effects of coastal vegetation zone width on wave run-up attenuation. Ocean Eng. 189, 106395 https://doi.org/10.1016/j.oceaneng.2019.106395.
Temmerman, S., Horstman, E.M., Krauss, K.W., Mullarney, J.C., Pelckmans, I., Schoutens, K., 2023. Marshes and mangroves as nature-based coastal storm buffers. Ann. Rev. Mar. Sci 15, 95–118. https://doi.org/10.1146/annurev-marine-040422-092951.
Teo, F.Y., Falconer, R.A., Lin, B., 2009. Modelling effects of mangroves on tsunamis. Proc. Inst. Civ. Eng. Water Manag. 162, 3–12. https://doi.org/10.1680/wama.2009.162.1.3.
Tomiczek, T., Asce, M., Donnell, K.O., Furman, K., Webbmartin, B., Scyphers, S., 2020a. Rapid damage assessments of shorelines and structures in the Florida keys after hurricane. Irma 21, 1–14. https://doi.org/10.1061/(ASCE)NH.1527-6996.0000349.
Tomiczek, T., Wargula, A., Cox, D.T., Lomónaco, P., Kelty, K., Ostrow, K., Chan, S., Mitchell, W., 2023. Wave height attenuation and damage reduction by mangrove forests: field and laboratory investigations. In: The Proceedings of the Coastal Sediments 2023, pp. 2630–2644. https://doi.org/10.1142/9789811275135_0240.
Tomiczek, T., Wargula, A., Lomónaco, P., Goodwin, S., Cox, D., Kennedy, A., Lynett, P., 2020b. Physical model investigation of mid-scale mangrove effects on flow hydrodynamics and pressures and loads in the built environment. Coast. Eng. 162 https://doi.org/10.1016/j.coastaleng.2020.103791.
Van Coppenolle, R., Schwarz, C., Temmerman, S., 2018. Contribution of mangroves and salt marshes to nature-based mitigation of coastal flood risks in major deltas of the world. Estuar. Coast 41, 1699–1711. https://doi.org/10.1007/s12237-018-0394-7.
van Hespen, R., Hu, Z., Peng, Y., Borsje, B.W., Kleinhans, M., Ysebaert, T., Bouma, T.J., 2021. Analysis of coastal storm damage resistance in successional mangrove species. Limnol. Oceanogr. 66, 3221–3236. https://doi.org/10.1002/lno.11875.
Veelen, T.J. Van, Fairchild, T.P., Reeve, D.E., Karunarathna, H., 2020. Experimental study on vegetation flexibility as control parameter for wave damping and velocity structure. Coast. Eng. 157, 103648 https://doi.org/10.1016/j.coastaleng.2020.103648.
Vuik, V., van Vuren, S., Borsje, B.W., van Wesenbeeck, B.K., Jonkman, S.N., 2018. Assessing safety of nature-based flood defenses: dealing with extremes and uncertainties. Coast. Eng. 139, 47–64. https://doi.org/10.1016/j.coastaleng.2018.05.002.
Wang, Y., Yin, Z., Liu, Y., 2022a. Laboratory study on the drag coefficient for mangrove forests in regular waves. Ocean Eng. 255, 111522 https://doi.org/10.1016/j.oceaneng.2022.111522.
Wang, Y., Yin, Z., Liu, Y., 2022b. Experimental investigation of wave attenuation and bulk drag coefficient in mangrove forest with complex root morphology. Appl. Ocean Res., 102974 https://doi.org/10.1016/j.apor.2021.102974.

Wang, Y., Yin, Z., Liu, Y., 2021. Predicting the bulk drag coefficient of flexible vegetation in wave flows based on a genetic programming algorithm. Ocean Eng. 223, 108694 https://doi.org/10.1016/j.oceaneng.2021.108694.

Weiss, M., Baret, F., Smith, G.J., Jonckheere, I., Coppin, P., 2004. Review of methods for in situ leaf area index (LAI) determination Part II. Estimation of LAI, errors and sampling 121, 37–53. https://doi.org/10.1016/j.agrformet.2003.08.001.

Wu, W., Cox, D.T., 2015. Effects of vertical variation in vegetation density on wave attenuation. J. Waterw. Port, Coast. Ocean Eng. 04015020. https://doi.org/10.1061/(ASCE)WW.1943-5460.0000326.

Wu, W.C., Cox, D.T., 2015. Effects of wave steepness and relative water depth on wave attenuation by emergent vegetation. Estuar. Coast Shelf Sci. 164, 443–450. https://doi.org/10.1016/j.ecss.2015.08.009.

Yanagisawa, H., Koshimura, S., Miyag, T., Imamura, F., 2010. Tsunami damage reduction performance of a mangrove forest in Banda Aceh, Indonesia inferred from field data and a numerical model. J. Geophys. Res. Ocean. 115, 1–11. https://doi.org/10.1029/2009JC005587.

Yuanita, N., Kurniawan, A., Muhamad, I., Maureza, F., 2021. A physical model simulation of combination of a geo-bag dike and mangrove vegetation as a natural coastal protection system for the Indonesian shoreline. Appl. Ocean Res. 108, 102516 https://doi.org/10.1016/j.apor.2020.102516.

Zhou, X., Dai, Z., Pang, W., Wang, J., Long, C., 2022. Wave attenuation over mangroves in the nanliu delta, China. Front. Mar. Sci. 9, 1–13. https://doi.org/10.3389/fmars.2022.874818.

Zhu, Z., Vuik, V., Visser, P.J., Soens, T., van Wesenbeeck, B., van de Koppel, J., Jonkman, S.N., Temmerman, S., Bouma, T.J., 2020. Historic storms and the hidden value of coastal wetlands for nature-based flood defence. Nat. Sustain. https://doi.org/10.1038/s41893-020-0556-z.